

University of Reading
School of Mathematics, Meteorology and Physics

Harbour modelling and resonances

Cassandra Moran

August 2008

This dissertation is submitted to the Department of Mathematics in partial fulfilment of the requirements for the degree of Master of Science.

Abstract

This dissertation considers the behaviour of water waves within a harbour. The problem is motivated by both real world applications as well as being of interest from a purely abstract mathematical perspective. The harbour is modelled as a simple rectangular domain which is partially open on one side to the ocean. Techniques used in previous work on wave diffraction around a breakwater are adopted, and Partial Differential Equation and Integral Equation methods are used to formulate the equations describing the wave field within and outside of the harbour.

The governing integral equation that is formed is solved numerically using Galerkin's method, and graphical representations of the wave field are plotted. The effects of variations in the angle of the incident wave, and the wave number are analysed. In particular the phenomenon of harbour resonance is investigated, focusing on what wave numbers cause a resonant effect, but also examining the effect of changes in the incident wave angle, the size of the opening onto the ocean, and the dimensions of the harbour.

Acknowledgements

Firstly I would like to thank my supervisors: Pete Chamberlain for his endless supply of ideas, enthusiasm and encouragement; and Nick Biggs for the same, and in particular for holding my hand on all the occasions when my program went wrong.

As always thanks go to my parents for their endless support, and giving me the courage to take a leap of faith this year.

To the 105 gang, thank you for trying to keep me sane through the last month, and for reminding me of the importance of being silly. It's been a fantastic if crazy year.

Thank you Mog - you know why.

Finally I would like to acknowledge the EPSRC for their financial support for this MSc course.

Declaration

I confirm that this is my own work, and the use of all material from other sources has been properly and fully acknowledged.

Signed Date

Contents

1	Introduction	1
2	Background	4
2.1	The previous literature	4
2.2	The breakwater problem	5
2.2.1	The scenario	5
2.2.2	Boundary conditions	6
2.2.3	Method of solution	8
2.2.4	Comparison to the harbour problem	9
3	Formulating the harbour problem	10
3.1	The scenario	10
3.2	Formulating the problem inside the harbour	11
3.3	Formulating the problem outside the harbour	15
3.4	The whole picture	17
3.5	The special case for $\alpha_m b = w\pi$	18
4	Solving the integral equation	21
4.1	Finding the weak form of the equation	21
4.2	Dealing with the singularities on the left hand side of (4.8)	23
4.2.1	The Hankel function	24
4.2.2	The sum of trigonometric functions	27
4.3	The Asymmetric case: adapting the integral equation	30
4.3.1	The right hand side of (4.8)	31
4.3.2	The left hand side of (4.8)	31

5	Programming a solution method	33
5.1	Programming the Galerkin method	33
5.2	Singularities	34
5.3	Checks for convergence	36
5.3.1	The breakwater problem	37
5.3.2	The full harbour problem	38
6	Results	40
6.1	Interpretation of the graph plots	40
6.2	Continuity over the gap	41
6.3	The effect of changing k , β and g	43
6.3.1	Altering k and β	43
6.3.2	Altering g	45
7	Resonance	47
7.1	Finding a suitable value of k	47
7.2	Maximising the effect of β	48
7.3	Results	49
7.3.1	A resonant case in the harbour	49
7.3.2	The effect of varying C and D	52
7.3.3	The effect of β on resonance	53
7.3.4	The size of the harbour	54
7.3.5	Changing the gap in the harbour mouth	55
7.3.6	The value of k	55
8	Conclusions	58
8.1	Summary	58
8.2	Future work	59
8.2.1	The asymmetric gap	59
8.2.2	The harbour	59
8.2.3	The coastal wall	59
8.3	Conclusions	60

List of Figures

1.1	Mullion harbour, Cornwall and West Bay, Bridport	1
1.2	Ciudadella harbour, Spain, 15 June 2006 [3]	2
2.1	View of the breakwater model from above	5
3.1	View of the harbour model from above	11
3.2	View of the harbour model from above	16
6.1	Exemplar plot.	40
6.2	Incident wave at an angle $\beta = \pi/4$, and frequency $k = 1$, zooming in on the gap. . . .	41
6.3	Slices parallel to the y axis checking for continuity over the gap for $k = 1$ and $\beta = \pi/4$, with $x = -0.4, 0$ and 0.4 respectively.	42
6.4	Slice parallel to the x axis checking for continuity over the gap for $k = 1$ and $\beta = \pi/4$	43
6.5	Incident wave at an angle $\beta = \pi/2$, and wave numbers $k = 1, 2, 3$ and 4 respectively. . . .	44
6.6	Incident wave at an angle $\beta = \pi/3$, and wave numbers $k = 1, 2, 3$ and 4 respectively. . . .	44
6.7	Incident wave at an angle $\beta = \pi/4$, and wave numbers $k = 1, 2, 3$ and 4 respectively. . . .	44
6.8	Incident wave at an angle $\beta = \pi/5$, and wave numbers $k = 1, 2, 3$ and 4 respectively. . . .	45
6.9	Incident wave at an angle $\beta = \pi/6$, and wave numbers $k = 1, 2, 3$ and 4 respectively. . . .	45
6.10	Incident wave at an angle $\beta = \pi/2$, wave number $k = 2$ and with $g = 0.05, 0.35, 0.65$ and 0.95 respectively.	46
6.11	Incident wave at an angle $\beta = \pi/3$, wave number $k = 2$ and with $g = 0.05, 0.35, 0.65$ and 0.95 respectively.	46
7.1	Plots of the real and imaginary solution respectively with $C = 4$ and $D = 3$	50
7.2	Plots of $\text{Im}(\phi)$ showing resonant response in the harbour, with $C = 1$ and $D = 1, 3, 5$ respectively.	51

7.3	Plots of $\text{Im}(\phi)$ showing resonant response in the harbour, with $C = 4$ and $D = 1, 3$ respectively.	51
7.4	Plots of the maximum value of $\text{Re}(\phi)$ within the harbour for $g = 0.05$ and $g = 0.1$, as C and D vary.	52
7.5	Plot of the maximum value of $\text{Im}(\phi)$ within the harbour for $g = 0.05$ and $g = 0.1$, as C and D vary.	53
7.6	Plot of the effect of varying β on maximum wave heights	53
7.7	Plot of the effect of varying the harbour width on maximum wave heights	54
7.8	Plot of the effect of varying the size of the gap on maximum wave heights	55
7.9	Plot of the effect of varying k on maximum wave heights	56
7.10	Focused plot of the effect of varying k on maximum wave heights.	57
8.1	Plot of $\text{Re}(\phi)$ showing resonant response in the harbour, with $k = 14.05$ and $\beta = \pi/20$	61

List of Tables

- 5.1 Results for the breakwater problem. 37
- 5.2 Linton & McIver’s results with the Galerkin method. 38
- 5.3 Checking for convergence with the Galerkin method for varying values of P , keeping
 $J = 80$ 39
- 5.4 Checking for convergence in the sum term for varying values of J , keeping $P = 10$. . . 39

- 7.1 Ranges of k where resonance occurs. 56

- 1 Values of k given various values of C and D 62

Chapter 1

Introduction

The aim of this project is to examine the behaviour of water waves within a harbour, in particular investigating the phenomena of harbour resonances. The engineering of harbour design is highly dependent on the behaviour of water waves within a harbour. It has to provide both defensive walls against flooding, and also safe mooring for boats.

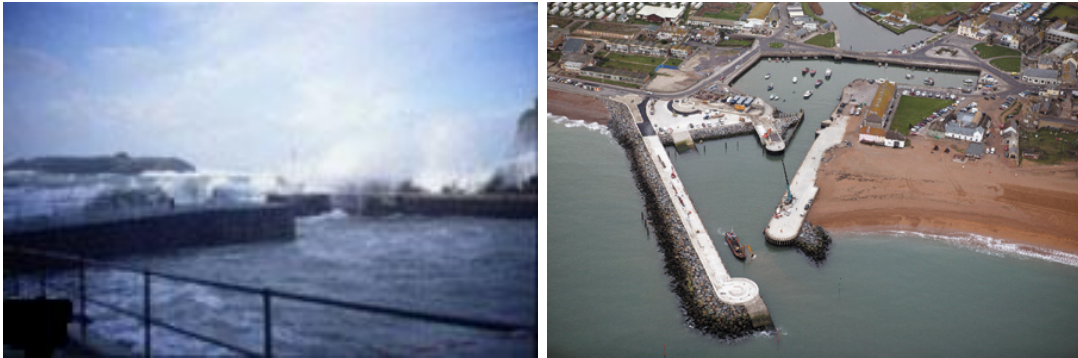


Figure 1.1: Mullion harbour, Cornwall and West Bay, Bridport

Harbour resonance is a particular issue as relatively small harbour oscillations can cause considerable damage to ships that are moored. This phenomenon is called a seiche, which is a standing wave oscillation of an enclosed water body, such as a lake, bay, harbour

(or bathtub!) It acts in a pendulum fashion even after the original causative force has ended (Scripps Institution of Oceanography, UC San Diego [4]). According to Jansa, Monserrat and Gomis [3], “*every port, bay or inlet has a natural oscillation mode or seiche with a period determined by the physical characteristics of the water body...Natural seiches usually have very small amplitude (of the order of a few centimetres at most) and can hardly be visually detected. They appear when the body water oscillates around the equilibrium after some small perturbation. However, sometimes they can reach large amplitudes when they are amplified due to resonance with an external exciter.*”

An example of such an occurrence is the rissaga (local name for a seiche) at Ciutadella Harbour in Spain. Here the rissaga occurs several times a year, mostly in the summer, and is generally approximately one metre in amplitude, and lasts around 10 minutes [3]. However on 15 June 2006 a rissaga of roughly five metres amplitude occurred, resulting in damage to many boats within the harbour.



Figure 1.2: Ciutadella harbour, Spain, 15 June 2006 [3]

Figure 1.2 shows the effect of this event as the water rapidly changes in height within the harbour leaving boats suddenly beached, and then pulled off their moorings/anchorage and flung against the harbour walls. While seiches are often caused by dramatic atmospheric or seismic events such as earthquakes or atmospheric pressures oscillations, they can however be brought about by simple tidal action - if this is at the specific frequency that will cause resonance.

In Chapter 2 we shall discuss the work on water wave diffraction through breakwaters that has been done by Porter [1] and Linton & McIver [2]. This will be used in Chapter 3 to guide our approach to formulating the equations that describe the wave behaviour both inside and outside of the harbour. We shall be using Partial Differential Equation (PDE) and Integral Equation methods in order to model a simple rectangular domain, that is partially open to the ocean. Equations will be set up to describe the wave field inside and outside of the harbour, and these will then be matched at the harbour mouth where they meet.

We then go on to look at our chosen method of solution, the Galerkin method, in Chapter 4. We will discuss how to deal with singularities that occur in the integral equation in question, and also how to adapt the method to cope with an asymmetric opening to the ocean. In Chapter 5 the process of writing a program in Matlab to numerically solve the integral equation will be described, and evidence of convergence in the program's results will be discussed.

The results for a basic model of the harbour, varying wave numbers and angles for the incident wave, will then be shown and discussed in Chapter 6. This will then be followed up in Chapter 7 with a look at the case where resonance occurs. In particular we shall be exploring what wave number produces a resonant effect, and whether the angle of the incident wave, the dimensions of the harbour, and the width of the gap in the harbour mouth have any impact on this resonance.

In Chapter 8 we shall then summarise our conclusions, and discuss some of the further paths of enquiry remain for the future.

Chapter 2

Background

In this chapter we will discuss some of the literature relevant to the harbour modelling problem, and look at the mathematical processes from this literature that can be adapted and used in solving the harbour problem.

2.1 The previous literature

The two main works that are referred to in this project are Porter's *Wave diffraction around breakwaters* [1] and *Handbook of Mathematical Techniques for Wave/Structure Interactions* by Linton & McIver [2].

In Porter's work [1] a number of scenarios involving breakwaters are addressed in order to develop the use of methods involving integral equations. The most relevant scenario is a model looking at an infinite, straight breakwater with a gap. In Linton & McIver's work [2] Chapter 4.7 also deals with diffraction of waves by a breakwater in order to illustrate integral equation methods. The formulation and solution of the breakwater problem is similar to that of the harbour problem looked at in this project, and therefore a number of techniques used by both [1] and [2] will be adopted.

The breakwater problem is therefore described in Section 2.2 below, before going on to set up the harbour problem in the following chapter.

2.2 The breakwater problem

2.2.1 The scenario

The breakwater is modelled as a solid, infinite, straight rectangular wedge of thickness $2d$, with a gap of width $2b$. The origin is placed so that it is at the centre of the gap as shown in Figure 2.1 below. An incident wave is then prescribed which hits the breakwater at an angle α to the outer wall of the breakwater, and is partly reflected and partly diffracted by it. To simplify the model it is assumed that the breakwater is perfectly reflecting, and that the water is inviscid, incompressible, homogeneous and in irrotational motion.

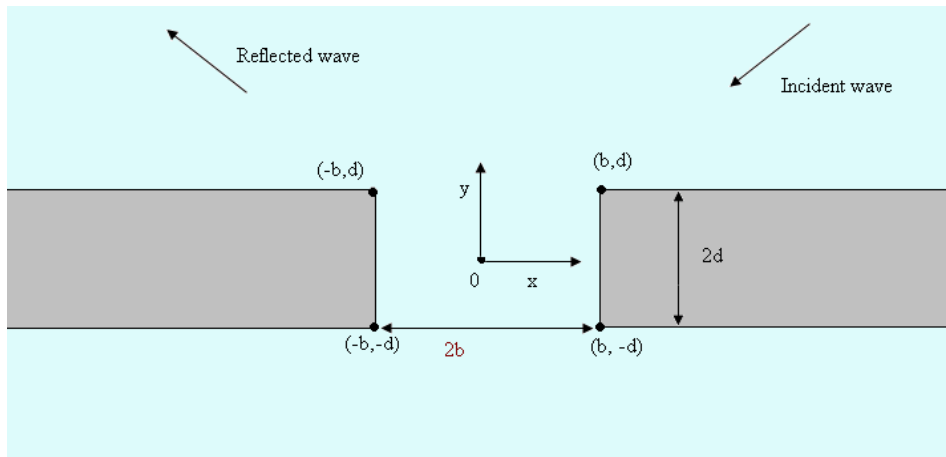


Figure 2.1: View of the breakwater model from above

Since irrotational flow is assumed, and therefore the velocity field \mathbf{q} satisfies $\nabla \times \mathbf{q} = 0$, we can write $\mathbf{q} = -\nabla\Phi$ where the potential function $\Phi(x, y, z, t)$ satisfies Laplace's equation. We can eliminate dependence on the vertical space variable z and time t by setting Φ as

$$\Phi = \operatorname{Re} \left\{ \frac{g \cosh k(z+h)}{i\sigma \cosh(kh)} \phi(x, y) e^{-i\sigma t} \right\} \quad (2.1)$$

where σ is the imposed wave frequency, z is measured vertically upwards with $z = 0$ at the undisturbed free surface and $z = -h$ at the sea bed, and the local wave number k is given by the dispersion relation

$$\sigma^2 = gk \tanh(kh). \quad (2.2)$$

If Φ is substituted into Laplace's equation, the equation reduces to the Helmholtz equation in terms of ϕ ,

$$\phi_{xx} + \phi_{yy} + k^2\phi = 0. \quad (2.3)$$

The solution $\phi(x, y)$ is made up of different components and we may write these as follows

$$\begin{aligned} \phi(x, y) &= \phi_i(x, y) + \phi_r(x, y) + \phi_d(x, y), & y > d, -\infty < x < \infty \\ &= \phi_d(x, y), & |y| < d, |x| < b, \text{ and} \\ & & y < -d, -\infty < x < \infty \end{aligned} \quad (2.4)$$

where ϕ_i is the incident wave, ϕ_r is the reflected wave and ϕ_d is the diffracted wave. The incident wave can be represented by

$$\phi_i(x, y) = Ae^{ikds\sin\alpha - ik(x\cos\alpha + y\sin\alpha)} \quad (2.5)$$

where A is a prescribed amplitude. The reflected wave component is represented by

$$\phi_r(x, y) = Ae^{-ikds\sin\alpha - ik(x\cos\alpha - y\sin\alpha)}. \quad (2.6)$$

2.2.2 Boundary conditions

There are a number of conditions that need to be satisfied. At the corners of the breakwater, derivatives cannot exist, so an edge condition is specified in order to avoid source-like behaviour. Therefore the requirement that

$$\frac{\partial\phi}{\partial r} \approx r^{-\delta}, \quad r \rightarrow 0, \delta < 1 \quad (2.7)$$

where r is the radial distance from the corners of the breakwater, is imposed. Considering the breakwater as a wedge of angle θ , then for $\theta < \pi$ this gives

$$\delta = \frac{(\pi - \theta)}{(2\pi - \theta)}. \quad (2.8)$$

The Sommerfeld radiation condition

$$\lim_{r \rightarrow \infty} r^{\frac{1}{2}} \left(\frac{\partial}{\partial r} - ik \right) \phi_d = 0 \quad (2.9)$$

where $r = \sqrt{x^2 + y^2}$, must also be satisfied uniformly in θ in order to ensure that the diffracted wave decays in the far-field. The diffracted wave ϕ_d must also satisfy the Helmholtz equation (2.3), the boundary conditions:

$$\left. \begin{aligned} \frac{\partial \phi_d}{\partial y} &= 0, \quad y = \pm d, \quad |x| < b \\ \frac{\partial \phi_d}{\partial x} &= 0, \quad x = \pm b, \quad |y| < d \end{aligned} \right\} \quad (2.10)$$

and also the jump conditions

$$\left. \begin{aligned} \phi_d(x, d+0) - \phi_d(x, d-0) &= -2Ae^{-ikx\cos\alpha} \\ \phi_d(x, -d+0) - \phi_d(x, -d-0) &= 0 \\ \phi_{d_y}(x, d+0) - \phi_{d_y}(x, d-0) &= 0 \\ \phi_{d_y}(x, -d+0) - \phi_{d_y}(x, -d-0) &= 0 \quad \text{for } |x| < b \end{aligned} \right\} \quad (2.11)$$

which ensure continuity of surface elevation and fluid velocity across $y = \pm d, |x| < b$.

2.2.3 Method of solution

Green's formula is used to convert the governing PDE into a pair of integral equations. Green's formula states that

$$\begin{aligned} \oint_C \left\{ \phi(x_0, y_0) \frac{\partial}{\partial n_0} G(x, y | x_0, y_0) - G(x, y | x_0, y_0) \frac{\partial}{\partial n_0} \phi(x_0, y_0) \right\} dC_0 \\ = \left\{ \begin{array}{l} \phi(x, y) \text{ if } (x, y) \in D \\ \frac{1}{2} \phi(x, y) \text{ if } (x, y) \in C \\ 0 \text{ if } (x, y) \notin D + C \end{array} \right\} \end{aligned} \quad (2.12)$$

where D is the domain, C the surrounding boundary, and n_0 the normal to the boundary C . Here the Green's function $G(x, y | x_0, y_0)$ is a solution of

$$(\nabla^2 + k^2)G = -\delta(x - x_0)\delta(y - y_0) \quad (2.13)$$

so that

$$G \approx -\frac{1}{2\pi} \log R \quad \text{as} \quad R = \sqrt{(x - x_0)^2 + (y - y_0)^2} \rightarrow 0. \quad (2.14)$$

An important solution is therefore

$$G_0 = \frac{1}{4} i H_0^{(1)}(kR) \quad (2.15)$$

where $H_0^{(1)}$ is the Hankel function of the first kind, of order zero given by

$$H_0^{(1)}(x) = J_0(x) + iY_0(x) \quad (2.16)$$

where $J_0(x)$ is a Bessel function of the first kind and $Y_0(x)$ is a Bessel function of the second kind which is singular at the origin. Both Bessel functions exhibit oscillatory and decaying behaviour.

The boundary value problem for ϕ_d at this point is completely stated, and is then converted into integral equations. Porter [1] uses the breakwater symmetry, to produce two independent integral equations, one for the symmetric part and one for the anti-symmetric part. A variational method is then applied to obtain a numerical solution.

In Linton and McIver's work [2] a very similar process is used to set up the breakwater problem. However as they deal with the special case of thin barrier problem ($d = 0$), only one integral equation is constructed by matching the solution above and below the breakwater. They then use both a collocation process, and a Galerkin method to solve this integral equation.

2.2.4 Comparison to the harbour problem

The breakwater problem has a number of similarities to the harbour modelling problem that will be studied in this dissertation. The initial set-up of the problem is similar, in that the simplifying assumptions relating to the fluid and the breakwater walls, referred to in Section 2.2.1 still apply. There are only two regions - within and outside of the harbour - in the new problem rather than the three of the breakwater problem (above and below the breakwater, and within the gap). However the overall solution can still be split up into the same two components as modelled in (2.4) with an incident wave coming in at angle β to the coast, reflected waves travelling away at an angle $\pi - \beta$ to the coast, and diffracted waves created by the area within the harbour.

A boundary value problem then needs to be set up, just as within the breakwater problem and formulated into an integral equation which can be solved numerically. However in the harbour modelling problem, the solution within the harbour will be set up using separation of variables as an alternative to using Green's function. Linton and McIver's approach of matching the solution within and outside of the harbour will be followed since the coastal walls will be treated as thin. This will then be solved numerically using Galerkin's method.

Chapter 3

Formulating the harbour problem

In this chapter, we shall describe the harbour modelling problem in detail, and set up the relevant equations that need to be solved. This will be done separately for the wave field inside and outside the harbour. These two sets of equations will then be matched to produce an integral equation that needs to be solved.

3.1 The scenario

The harbour is modelled as a rectangular domain of width $2a$ and length b , with the origin placed in the centre of the harbour mouth. The coastal wall extends across the entrance to the harbour, as shown in Figure 3.1 below, so that the harbour mouth is of width $2g \in (0, 2a)$. The gap is not extended to reach exactly $2a$ as this would affect the corner condition that is applied and require a slightly different computational approach. The wall and gap are kept symmetric, though at a later point the adjustments needed to model asymmetry will be discussed. The wall is modelled as infinitely thin.

An incident wave comes towards the harbour at an angle β to the coast. Where this hits the coastal wall, it will be perfectly reflected back out to sea at an angle $\pi - \beta$, and where it is able to travel through the harbour mouth, it will be diffracted. Therefore within the harbour, the wave solution is made up solely of the diffracted wave ϕ_d^- and outside the harbour the wave solution is the sum of the incident, reflected and diffracted

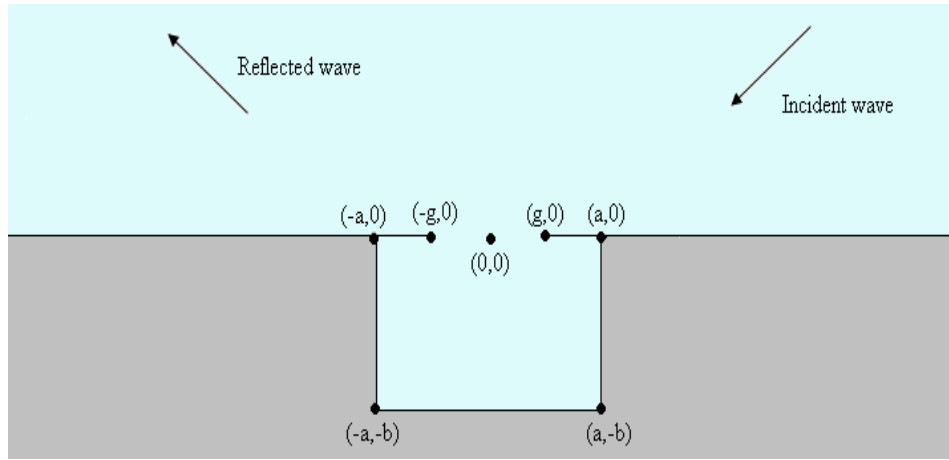


Figure 3.1: View of the harbour model from above

waves: $\phi_i + \phi_r + \phi_d^+$ where

$$\phi_i = Ae^{-ik(x \cos \beta + y \sin \beta)} \quad (3.1)$$

and

$$\phi_r = Ae^{-ik(x \cos \beta - y \sin \beta)}. \quad (3.2)$$

3.2 Formulating the problem inside the harbour

Within the harbour in order to model the assumption that the walls are solid and perfectly reflecting, the relevant boundary conditions are that

$$\begin{aligned} \frac{\partial \phi_d^-}{\partial x} &= 0, \quad x = \pm a, \quad -b < y < 0 \\ \frac{\partial \phi_d^-}{\partial y} &= 0, \quad y = -b, \quad |x| < a \\ \frac{\partial \phi_d^-}{\partial y} &= 0, \quad y = 0, \quad -a < x < -g \quad \text{and} \quad g < x < a. \end{aligned} \quad (3.3)$$

As discussed in Chapter 2, the Helmholtz equation

$$\phi_{xx} + \phi_{yy} + k^2 \phi = 0 \quad (3.4)$$

needs to be solved for the diffracted wave in the harbour area, and this will be done with the method of separation of variables. If we let

$$\phi_d^-(x, y) = X(x)Y(y) \quad (3.5)$$

then substituting this into the Helmholtz equation (3.4) and re-arranging we get

$$\begin{aligned} X''Y + XY'' + k^2XY &= 0 \\ \Rightarrow \frac{X''}{X} = -\frac{Y''}{Y} - k^2 &= -\lambda^2 \end{aligned} \quad (3.6)$$

which implies that

$$\begin{aligned} X'' + \lambda^2X &= 0, \\ Y'' + (k^2 - \lambda^2)Y &= 0, \end{aligned} \quad (3.7)$$

where λ is the separation constant. This leads to the general solution for X of

$$X = A\cos[\lambda(x + a)] + B\sin[\lambda(x + a)]. \quad (3.8)$$

The boundary conditions (3.3) then need to be applied to find the particular solution. These imply that $X'(-a) = 0$, so $B = 0$, and also $X'(a) = 0$, so that either $A = 0$ or else $\lambda = \lambda_n = \frac{n\pi}{2a}$, for $n \in \mathbb{N} \cup \{0\}$. We therefore have the particular solutions for X

$$X_n = A_n \cos \left[\frac{n\pi}{2a}(x + a) \right], \quad n \in \mathbb{N} \cup \{0\}, \quad (3.9)$$

and can perform a similar process to solve for Y . From (3.7) we have that

$$Y_n'' + (k^2 - \lambda_n^2)Y_n = 0, \quad n \in \mathbb{N} \cup \{0\}. \quad (3.10)$$

For ease of notation if we now let

$$\alpha_n^2 = k^2 - \lambda_n^2 \quad (3.11)$$

which gives us a value of

$$\alpha_n = \begin{cases} \sqrt{k^2 - \lambda_n^2} & k > \lambda_n \\ i\sqrt{\lambda_n^2 - k^2} & k < \lambda_n \end{cases} \quad (3.12)$$

then this leads to the general solution for Y_n of

$$Y_n = C_n \cos[\alpha_n(y + b)] + D_n \sin[\alpha_n(y + b)]. \quad (3.13)$$

Similarly to before, using the derivative boundary conditions (3.3) gives $Y'_n(-b) = 0$, so $D_n = 0$, and

$$Y_n = C_n \cos[\alpha_n(y + b)]. \quad (3.14)$$

Using (3.5) then gives ϕ_d^- as

$$\phi_d^- = \sum_{n=0}^{\infty} f_n \cos\left[\frac{n\pi}{2a}(x + a)\right] \cos[\alpha_n(y + b)]. \quad (3.15)$$

In order to find the unknown constants f_n we use a Fourier series approach, initially differentiating with respect to y , and putting $y = 0$,

$$\frac{\partial \phi_d}{\partial y}(x, 0) = \sum_{n=0}^{\infty} -f_n \alpha_n \cos\left[\frac{n\pi}{2a}(x + a)\right] \sin[\alpha_n b]. \quad (3.16)$$

Then by integrating both sides with respect to x , multiplying by a cos term and then

using properties of orthogonality we can find that

$$\begin{aligned} & \int_{-a}^a \frac{\partial \phi_d}{\partial y}(x, 0) \cos \left[\frac{m\pi}{2a}(x+a) \right] dx \\ &= \sum_{n=0}^{\infty} -f_n \alpha_n \sin[\alpha_n b] \int_{-a}^a \cos \left[\frac{m\pi}{2a}(x+a) \right] \cos \left[\frac{n\pi}{2a}(x+a) \right] dx \\ &= \begin{cases} 0 & \text{for } m \neq n, \\ -a \epsilon_n f_n \alpha_n \sin[\alpha_n b] & \text{for } m = n, \end{cases} \end{aligned} \quad (3.17)$$

where

$$\epsilon_n = \begin{cases} 2 & n = 0, \\ 1 & n \geq 1. \end{cases} \quad (3.18)$$

So the solution for the diffracted wave within the harbour is

$$\phi_d^- = \sum_{n=0}^{\infty} \left\{ -\frac{\cos \left[\frac{n\pi}{2a}(x+a) \right] \cos[\alpha_n(y+b)]}{a \epsilon_n \alpha_n \sin(\alpha_n b)} \int_{-a}^a \frac{\partial \phi_d}{\partial y}(x_0, 0^-) \cos \left[\frac{n\pi}{2a}(x_0+a) \right] dx_0 \right\} \quad (3.19)$$

which can be written as

$$\phi_d^- = \int_{-g}^g \frac{\partial \phi_d}{\partial y}(x_0, 0^-) \left[\sum_{n=0}^{\infty} \frac{-\cos[\lambda_n(x_0+a)] \cos[\lambda_n(x+a)] \cos[\alpha_n(y+b)]}{a \epsilon_n \alpha_n \sin(\alpha_n b)} \right] dx_0. \quad (3.20)$$

The integration boundaries have been altered from the maximum harbour gap of $-a$ to a , to the gap that is defined by g . This can be done since on the coastal wall $\frac{\partial \phi_d}{\partial y}(x_0, 0) = 0$, so there will only be a non-zero result from the integral within the ranges $(-a, -g)$ and (g, a) .

There is a possibility that for particular values of a , b and k , $\alpha_n b$ may be an exact multiple of π , leading to a zero denominator in the kernel of this integral. This case will be dealt with in Section 3.5 and for the time being we suppose that $\frac{\alpha_n b}{\pi} \in \mathbb{Z}$.

3.3 Formulating the problem outside the harbour

The Helmholtz equation (3.4) again needs to be solved for the diffracted wave in this region. This can then be combined with the incident and reflected waves to construct the full solution outside the harbour. A Green's function approach will be used to solve for the diffracted wave rather than separation of variables as used inside the harbour since this is an unbounded domain.

The diffracted wave needs to satisfy the Sommerfeld radiation condition which ensures that waves decay in the far field. This is

$$\lim_{r \rightarrow \infty} r^{\frac{1}{2}} \left(\frac{\partial}{\partial r} - ik \right) \phi_d^+ = 0, \quad r^2 = x^2 + y^2 \quad (3.21)$$

uniformly in θ , as well as the boundary condition that models the coastal wall as solid and perfectly reflecting, namely

$$\frac{\partial \phi_d^+}{\partial y} = 0, \quad |x| > a, \quad y = 0^+. \quad (3.22)$$

Applying Green's formula we let $G(x, y|x_0, y_0)$ satisfy

$$\begin{aligned} \nabla^2 G + k^2 G &= -\delta(x - x_0)\delta(y - y_0) \text{ in } D \\ \frac{\partial G}{\partial y} &= 0, \quad y = 0 \end{aligned} \quad (3.23)$$

where D represents the semi-circular finite domain, with centre at the origin as shown in Figure 3.2 below, and C represents the edge of the domain D . G must also satisfy the Sommerfeld radiation condition as stated in (3.21).

Then by applying Green's identity in conjunction with the boundary conditions (3.22)

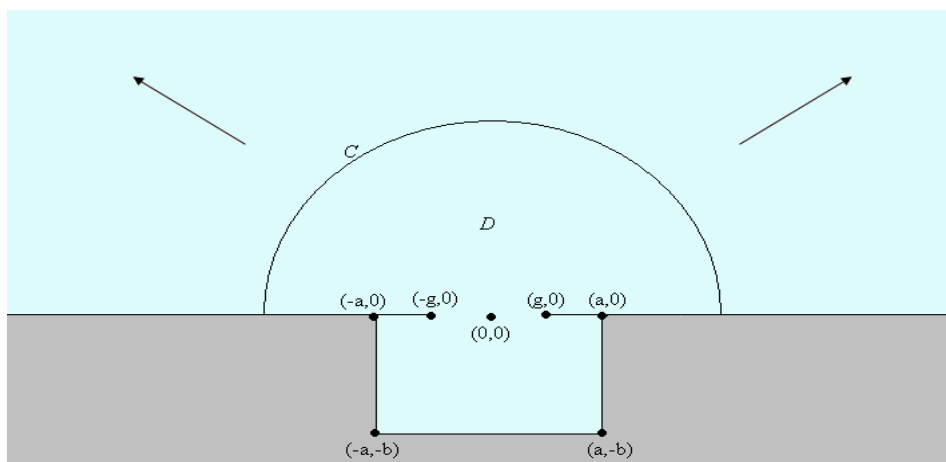


Figure 3.2: View of the harbour model from above

and (3.23) we get

$$\begin{aligned}
\int \int_D \phi_d^+ \nabla^2 G - G \nabla^2 \phi_d^+ dx dy &= \int \int_D \phi_d^+ (\nabla^2 G + k^2 G) - G (\nabla^2 \phi_d^+ + k^2 \phi_d^+) dx dy \\
&= \oint_C \phi_d^+ \frac{\partial G}{\partial n} - G \frac{\partial \phi_d^+}{\partial n} dC \\
&= \int_{\text{gap}} \phi_d^+ \frac{\partial G}{\partial y} + G \frac{\partial \phi_d^+}{\partial y} dx \\
&\quad + \int_{\text{coast}} \phi_d^+ \frac{\partial G}{\partial y} + G \frac{\partial \phi_d^+}{\partial y} dx \\
&\quad + \int_{\text{far-field}} \phi_d^+ \frac{\partial G}{\partial r} + G \frac{\partial \phi_d^+}{\partial r} dr \\
&= \int_{\text{gap}} + G \frac{\partial \phi_d^+}{\partial y} dx
\end{aligned} \tag{3.24}$$

where \underline{n} is a normal and $\frac{\partial \phi}{\partial n} = \underline{n} \cdot \underline{\nabla} \phi$. Therefore the solution outside the harbour for the diffracted wave is of the form

$$\phi_d^+(x_0, y_0) = - \int_{\text{gap}} G|_{y=0} \frac{\partial \phi_d^+}{\partial y} |_{y=0} dx_0 \tag{3.25}$$

where G is based upon a Hankel function, which therefore decays for large x, y so satisfying the Sommerfeld radiation condition (3.21), and can be written in the following way using the method of images to ensure G satisfies the derivative boundary conditions (3.23):

$$G(x, y|x_0, y_0) = \frac{i}{4}[H_0^{(1)}(k\sqrt{\{(x-x_0)^2 + (y-y_0)^2\}}) + H_0^{(1)}(k\sqrt{\{(x-x_0)^2 + (y+y_0)^2\})}]. \quad (3.26)$$

The solution will also need to satisfy the edge condition as given in equations (2.7) and (2.8) with $\theta = 0$ for a thin wall. This means we require

$$\frac{\partial\phi}{\partial r} = O(r^{-\frac{1}{2}}) + o(r^{-\frac{1}{2}}) \quad (3.27)$$

around the corners of the harbour mouth. The effect of this condition can be seen in Section 4.2.

Across the harbour mouth (gap) the required Green's function therefore gives the solution for the diffracted wave as

$$\phi_d^+(x_0, 0^+) = -\frac{i}{2} \int_{\text{gap}} \frac{\partial\phi_d}{\partial y}(x, 0^+) H_0^{(1)}\{k|x-x_0|\} dx. \quad (3.28)$$

In order to match the notation for the expression within the harbour, x and x_0 are now interchanged. The complete solution outside the harbour, ϕ^+ , is then made up of the incident, reflected and diffracted waves:

$$\begin{aligned} \phi^+(x, y) = & A e^{-ik(x\cos\beta + y\sin\beta)} + A e^{-ik(x\cos\beta - y\sin\beta)} \\ & - \frac{i}{2} \int_{\text{gap}} \frac{\partial\phi_d}{\partial y}(x_0, 0^+) H_0^{(1)}\{k\sqrt{(x-x_0)^2 + y^2}\} dx_0. \end{aligned} \quad (3.29)$$

3.4 The whole picture

Across the gap in the harbour mouth, the solution for the diffracted wave within the harbour (3.20) has to match the total solution for the diffracted, incident and reflected

waves outside the harbour (3.29). Equating these two expressions gives the integral equation

$$2Ae^{-ikx\cos\beta} = \int_{\text{gap}} \frac{\partial\phi_d}{\partial y}(x_0, 0) \left[\frac{i}{2}H_0^{(1)}\{k|x-x_0|\} + \sum_{n=0}^{\infty} \frac{-\cos[\lambda_n(x_0+a)]\cos[\lambda_n(x+a)]\cos[\alpha_nb]}{a\epsilon_n\alpha_n\sin(\alpha_nb)} \right] dx_0 \quad (3.30)$$

which will then need to be solved for the unknown derivative $\frac{\partial\phi_d}{\partial y}(x_0, 0)$. Once this has been found, it can be substituted back into the two expressions for the solution inside (3.20) and outside (3.29) of the harbour, and this can then be plotted. For ease of notation, the derivative function $\frac{\partial\phi_d}{\partial y}(x_0, 0)$ will also be referred to as $v_\beta(x_0)$, and the kernel

$$\frac{i}{2}H_0^{(1)}\{k|x-x_0|\} + \sum_{n=0}^{\infty} \frac{-\cos[\lambda_n(x_0+a)]\cos[\lambda_n(x+a)]\cos[\alpha_nb]}{a\epsilon_n\alpha_n\sin(\alpha_nb)} \quad (3.31)$$

will be referred to as $K(x, x_0) = K^{(1)}(x, x_0) + K^{(2)}(x, x_0)$ with

$$K^{(1)}(x, x_0) = \frac{i}{2}H_0^{(1)}\{k|x-x_0|\} \quad (3.32)$$

and

$$K^{(2)}(x, x_0) = \sum_{n=0}^{\infty} \frac{-\cos[\lambda_n(x_0+a)]\cos[\lambda_n(x+a)]\cos[\alpha_nb]}{a\epsilon_n\alpha_n\sin(\alpha_nb)}. \quad (3.33)$$

The integral equation across the gap then becomes

$$2Ae^{-ikx\cos(\beta)} = \int_{-g}^g v_\beta(x_0)[K^{(1)}(x, x_0) + K^{(2)}(x, x_0)]dx_0. \quad (3.34)$$

3.5 The special case for $\alpha_m b = w\pi$

This case is also dealt with by Porter [1] for the breakwater problem and his solution can be directly applied to the harbour problem as follows. If for a particular set of values of a , b and k we let $\alpha_m b = w\pi$ where w is an integer, then the eigenfunction

$$\phi_d^{m-}(x, y) = \cos\left[\frac{m\pi}{2a}(x+a)\right] \cos\left[\frac{w\pi}{b}(y+b)\right] \quad (3.35)$$

which satisfies the boundary conditions

$$\begin{aligned}\frac{\partial \phi_d^{m-}}{\partial x} &= 0, \quad x = \pm a \\ \frac{\partial \phi_d^{m-}}{\partial y} &= 0, \quad y = -b\end{aligned}\tag{3.36}$$

now also satisfies

$$\frac{\partial \phi_d^{m-}}{\partial y} = 0, \quad y = 0.\tag{3.37}$$

The effect of $v_\beta(x_0) = 0$ in this case is that f_m cannot be found in equation (3.17) in the same way as before. However an arbitrary amount of $\phi_d^{m-}(x, y)$ may be included in $\phi_d^-(x, y)$ and the coefficient f_m determined by the continuity requirements of $\phi_d^-(x, y)$.

Since f_m cannot be related to $v_\beta(x_0)$, kernel $K^{(2)}(x, x_0)$ (3.33) needs to be modified by excluding the $n = m$ term in the integral equation (3.34), and by replacing it with

$$f_m \phi_d^{m-}(x, 0) = f_m \cos\left[\frac{m\pi}{2a}(x + a)\right] \cos(w\pi)\tag{3.38}$$

which is the $n = m$ term expressed without dependence on $v_\beta(x_0)$.

$$\begin{aligned}2Ae^{-ikx \cos(\beta)} &= \int_{-g}^g v_\beta(x_0)[K^{(1)}(x, x_0) + K^{(2)}(x, x_0)]dx_0 \\ &= \int_{-g}^g v_\beta(x_0)[K^{(1)}(x, x_0) + K^{(2)'}(x, x_0)] + v_\beta(x_0)K^{(n=m)}(x, x_0)dx_0 \\ &= \int_{-g}^g v_\beta(x_0)[K^{(1)}(x, x_0) + K^{(2)'}(x, x_0)]dx_0 + f_m \cos\left[\frac{m\pi}{2a}(x + a)\right] \cos(w\pi)\end{aligned}\tag{3.39}$$

where the kernel $K^{(2)}(x, x_0)$ is split up into $K^{(2)'}(x, x_0)$ without the $n = m$ case, and $K^{(n=m)}(x, x_0)$ being the $n = m$ case. Then since the integral equation is linear, $v_\beta(x_0)$ can be written in the form

$$v_\beta(x_0) = v_\beta^{(1)}(x_0) - f_m v_\beta^{(2)}(x_0)\tag{3.40}$$

where

$$\int_{-g}^g v_{\beta}^{(1)}(x_0)[K^{(1)}(x, x_0) + K^{(2)'}(x, x_0)]dx_0 = 2Ae^{-ikx \cos(\beta)} \quad (3.41)$$

$$\int_{-g}^g v_{\beta}^{(2)}(x_0)[K^{(1)}(x, x_0) + K^{(2)'}(x, x_0)]dx_0 = \cos\left[\frac{m\pi}{2a}(x + a)\right] \cos(w\pi). \quad (3.42)$$

Both $v_{\beta}(x_0)^{(1)}$ and $v_{\beta}(x_0)^{(2)}$ can then be solved for and since for $\sin(\alpha_m b) = 0$ equation (3.17) implies that

$$\int_{-g}^g v_{\beta}(x) \cos\left[\frac{m\pi}{2a}(x + a)\right]dx = 0 \quad (3.43)$$

then f_m can be evaluated by combining (3.43) and (3.40) to give

$$\int_{-g}^g v_{\beta}^{(1)}(x_0) \cos\left[\frac{m\pi}{2a}(x_0 + a)\right]dx_0 = f_m \int_{-g}^g v_{\beta}^{(2)}(x_0) \cos\left[\frac{m\pi}{2a}(x_0 + a)\right]dx_0. \quad (3.44)$$

Once f_m has been evaluated, it can be substituted back into equation (3.40) in order to find $v_{\beta}(x_0)$ and the waves inside and outside the harbour can be plotted as before.

Chapter 4

Solving the integral equation

In this chapter we shall examine the method of solution of the integral equation (3.34). In particular, since the kernel of the integral equation contains singularities, we shall look at how to remove these and deal with them analytically (in order to isolate the quantity remaining to be evaluated numerically).

4.1 Finding the weak form of the equation

In order to use the Galerkin method to solve this integral equation, we first write it in operator notation as

$$(\widehat{K}v_\beta)(x) = F_\beta(x), \text{ for } x \in (-g, g) \quad (4.1)$$

where $F_\beta(x) = 2Ae^{-ikx \cos(\beta)}$ and the operator \widehat{K} is given by

$$(\widehat{K}v_\beta)(x) = \int_{-g}^g K(x, x_0)v_\beta(x_0)dx_0. \quad (4.2)$$

An approximation $\tilde{v}_\beta(x_0) \approx v_\beta(x_0)$ is chosen by selecting a set of trial functions χ_l for ($l = 0 \dots P$) and approximating $v_\beta(x_0)$ with

$$\tilde{v}_\beta(x_0) = \sum_{p=0}^P t_p \chi_p. \quad (4.3)$$

The scalars t_p are to be determined with the requirement that the residual to the approximation is orthogonal to each of the trial functions, that is,

$$\langle \widehat{K}\tilde{v}_\beta - F_\beta, \chi_l \rangle = 0 \quad \text{for } l = 0, 1 \dots P \quad (4.4)$$

must be true, where the inner product is defined as

$$\langle f, h \rangle = \int_{-g}^g f(x)\bar{h}(x)dx. \quad (4.5)$$

The trial function needs to satisfy the edge condition $\frac{\partial\phi}{\partial r} \approx r^{-\frac{1}{2}}$ [see (2.7), (2.8) and (3.27)] around the corners of the harbour mouth. Therefore an appropriate choice is

$$\chi_l(x) = \frac{T_l\left(\frac{x}{g}\right)}{\sqrt{g^2 - x^2}}, \quad (4.6)$$

since this denominator will give the required value

$$\tilde{v}_\beta(x) \approx \begin{cases} (x+g)^{-\frac{1}{2}} & \text{as } x \rightarrow -g, \\ (g-x)^{-\frac{1}{2}} & \text{as } x \rightarrow g. \end{cases} \quad (4.7)$$

The numerator could be any function of x , but choosing it to be the Chebyshev polynomial of the first kind $T_l(x)$ allows a number of analytical simplifications in the following work. Putting the integral equation into the weak form with this choice of test function and approximation for $v_\beta(x_0)$ then gives

$$\sum_{p=0}^P t_p \langle \widehat{K}\chi_p, \chi_q \rangle = \langle F_\beta, \chi_q \rangle \quad \text{for } q = 0 \dots P \quad (4.8)$$

producing a set of $P + 1$ simultaneous equations to be solved, for the coefficients t_p .

By using the substitution $x = g \cos u$, the identity $T_n(x) = \cos(n \cos^{-1}(x))$ and an integral representation of the Bessel function (Abramowitz and Stegun [5] section 9.1.21),

the right hand side of (4.8) simplifies in the following way:

$$\begin{aligned}
 \langle F_\beta, \chi_q \rangle &= 2A \int_{-g}^g e^{-ikx \cos \beta} \frac{T_q\left(\frac{x}{g}\right)}{\sqrt{g^2 - x^2}} dx \\
 &= 2A \int_0^\pi e^{-ikg \cos u \cos \beta} \cos(qu) du \\
 &= 2A\pi(-i)^q J_q(kg \cos \beta),
 \end{aligned} \tag{4.9}$$

where J_q denotes a Bessel function of the first kind. On the left hand side of (4.8), we have

$$\begin{aligned}
 \langle \widehat{K} \chi_p, \chi_q \rangle &= \int_{-g}^g \int_{-g}^g \left\{ \frac{i}{2} H_0^{(1)}(k|x - x_0|) - \sum_{n=0}^{\infty} \frac{\cos[\lambda_n(x_0 + a)] \cos[\lambda_n(x + a)] \cos[\alpha_n b]}{a \epsilon_n \alpha_n \sin(\alpha_n b)} \right\} \\
 &\quad \times \left\{ \frac{T_p\left(\frac{x}{g}\right)}{\sqrt{g^2 - x^2}} \frac{T_q\left(\frac{x_0}{g}\right)}{\sqrt{g^2 - x_0^2}} \right\} dx dx_0
 \end{aligned} \tag{4.10}$$

which requires further analytical work before a numerical evaluation is attempted.

4.2 Dealing with the singularities on the left hand side of (4.8)

If we now define the following operator functions as

$$\begin{aligned}
 (\widehat{K}^{(1)} v_\beta)(x) &= \int_{-g}^g K^{(1)}(x, x_0) v_\beta(x_0) dx_0, \\
 (\widehat{K}^{(2)} v_\beta)(x) &= \int_{-g}^g K^{(2)}(x, x_0) v_\beta(x_0) dx_0
 \end{aligned} \tag{4.11}$$

then in both these terms there will be a singularity when $x = x_0$. This needs to be dealt with separately and evaluated analytically, whereas the rest of the equation can be evaluated numerically.

4.2.1 The Hankel function

First of all we will look at the term in equation (4.10) with the Hankel function, $\langle \widehat{K}^{(1)}\chi_p, \chi_q \rangle$, and having split this up into a non-singular and singular part, directly evaluate the latter. This process follows very closely that used by Linton & McIver [2] in their solution of the breakwater problem.

Using the substitutions $x = g\cos u$ and $x_0 = g\cos v$ the term in question becomes

$$\langle \widehat{K}^{(1)}\chi_p, \chi_q \rangle = \frac{i}{2} \int_0^\pi \int_0^\pi \left\{ H_0^{(1)}(kg|\cos u - \cos v|) \cos pu \cos qv \right\} du dv. \quad (4.12)$$

Depending on the values of p and q , this can be completely or partially evaluated analytically. If we apply the substitutions $u = \pi - u$ and $v = \pi - v$ in equation (4.12) the Hankel function term becomes:

$$\begin{aligned} & \langle \widehat{K}^{(1)}\chi_p, \chi_q \rangle \\ &= \frac{i}{2} \int_\pi^0 \int_\pi^0 \left\{ H_0^{(1)}(kg|\cos(\pi - u) - \cos(\pi - v)|) \cos p(\pi - u) \cos q(\pi - v) \right\} du dv \\ &= \frac{i}{2} \int_0^\pi \int_0^\pi \left\{ H_0^{(1)}(kg|\cos(u) - \cos(v)|) (-1)^p \cos(pu) (-1)^q \cos(qv) \right\} du dv. \end{aligned} \quad (4.13)$$

However when the sum of p and q is odd, (4.13) is equal to

$$-\frac{i}{2} \int_0^\pi \int_0^\pi \left\{ H_0^{(1)}(kg|\cos u - \cos v|) \cos pu \cos qv \right\} du dv = -\langle \widehat{K}^{(1)}\chi_p, \chi_q \rangle. \quad (4.14)$$

Therefore

$$\langle \widehat{K}^{(1)}\chi_p, \chi_q \rangle = 0 \quad \text{for } p + q \text{ odd.} \quad (4.15)$$

For other values of p and q , the expression for $\langle \widehat{K}^{(1)}\chi_p, \chi_q \rangle$ can be re-arranged in the following way, splitting up the Hankel function into its two constituent Bessel functions. Combined with the $\frac{i}{2}$ factor, this creates a non-singular imaginary part, and a real part with a singularity. However this singularity can be subtracted and added back on, in

order to isolate it from the remaining terms. Thus

$$\begin{aligned}
& \frac{i}{2} \int_0^\pi \int_0^\pi \left\{ H_0^{(1)}(kg|\cos u - \cos v|) \operatorname{cospucos} qv \right\} du dv \\
&= \int_0^\pi \int_0^\pi \left\{ \frac{i}{2} J_0(kg|\cos u - \cos v|) \operatorname{cospucos} qv - \frac{1}{2} Y_0(kg|\cos u - \cos v|) \operatorname{cospucos} qv \right\} du dv \\
&= \int_0^\pi \int_0^\pi \left\{ \frac{i}{2} J_0(kg|\cos u - \cos v|) \operatorname{cospucos} qv \right. \\
&\quad - \frac{1}{2} \left[Y_0(kg|\cos u - \cos v|) - \frac{2}{\pi} \ln|\cos u - \cos v| \right] \operatorname{cospucos} qv \\
&\quad \left. - \frac{1}{\pi} \ln|\cos u - \cos v| \operatorname{cospucos} qv \right\} du dv.
\end{aligned} \tag{4.16}$$

The first two terms of this expression are now smooth and so can be readily evaluated numerically, and the final term can be calculated as follows.

Using the identity from Appendix C of [7]

$$\ln[2|\cos A - \cos B|] = - \sum_{n=1}^{\infty} 2n^{-1} \cos(nA) \cos(nB) \quad (0 \leq A, B \leq \pi, A \neq B) \tag{4.17}$$

the final term can be re-written as

$$\begin{aligned}
& \int_0^\pi \int_0^\pi \ln|\cos u - \cos v| \operatorname{cospucos} qv du dv \\
&= \int_0^\pi \int_0^\pi \left[-\ln 2 - \sum_{r=1}^{\infty} 2r^{-1} \cos(ru) \cos(rv) \right] \operatorname{cospucos} qv du dv.
\end{aligned} \tag{4.18}$$

This expression then needs to be examined for different values of p and q . Once it has been evaluated, this value needs to be added back in after the remaining part of the Hankel function term has been calculated numerically.

For $p = q = 0$,

$$\begin{aligned}
& \int_0^\pi \int_0^\pi \left[-\ln 2 - \sum_{r=1}^{\infty} 2r^{-1} \cos(ru) \cos(rv) \right] \cos pu \cos qv \, du \, dv \\
&= \int_0^\pi \int_0^\pi \left[-\ln 2 - \sum_{r=1}^{\infty} 2r^{-1} \cos(ru) \cos(rv) \right] \, du \, dv \\
&= \int_0^\pi \int_0^\pi -\ln 2 \, du \, dv - \sum_{r=1}^{\infty} 2r^{-1} \int_0^\pi \cos(ru) \, du \int_0^\pi \cos(rv) \, dv \\
&= -\pi^2 \ln 2.
\end{aligned} \tag{4.19}$$

For $p \neq q$,

$$\begin{aligned}
& \int_0^\pi \int_0^\pi \left[-\ln 2 - \sum_{r=1}^{\infty} 2r^{-1} \cos(ru) \cos(rv) \right] \cos pu \cos qv \, du \, dv \\
&= -\ln 2 \int_0^\pi \cos(pu) \, du \int_0^\pi \cos(qv) \, dv - \sum_{r=1, r \neq p, q}^{\infty} 2r^{-1} \int_0^\pi \cos(ru) \cos pu \, du \int_0^\pi \cos(rv) \cos qv \, dv \\
&\quad - 2p^{-1} \int_0^\pi \cos^2 pu \, du \int_0^\pi \cos(pv) \cos qv \, dv - 2q^{-1} \int_0^\pi \cos(qu) \cos pu \, du \int_0^\pi \cos^2 qv \, dv \\
&= 0.
\end{aligned} \tag{4.20}$$

Lastly for $p = q \neq 0$,

$$\begin{aligned}
& \int_0^\pi \int_0^\pi \left[-\ln 2 - \sum_{r=1}^{\infty} 2r^{-1} \cos(ru) \cos(rv) \right] \cos pu \cos qv \, du \, dv \\
&= -\ln 2 \int_0^\pi \cos(pu) \, du \int_0^\pi \cos(pv) \, dv - \sum_{r=1, r \neq p}^{\infty} 2r^{-1} \int_0^\pi \cos(ru) \cos pu \, du \int_0^\pi \cos(rv) \cos pv \, dv \\
&\quad - 2p^{-1} \int_0^\pi \cos^2 pu \, du \int_0^\pi \cos^2(pv) \, dv \\
&= -\frac{\pi^2}{2p}.
\end{aligned} \tag{4.21}$$

We therefore now have

$$\begin{aligned}
& \langle \widehat{K}^{(1)} \chi_p, \chi_q \rangle \\
&= \frac{i}{2} \int_0^\pi \int_0^\pi \left\{ \left[H_0^{(1)}(kg|\cos u - \cos v|) - \frac{2}{\pi} \ln |\cos u - \cos v| \right] \cos p u \cos q v \right\} du dv \\
&+ \begin{cases} \pi \ln 2 & p = q = 0, \\ \frac{\pi}{2p} & p = q \neq 0, \\ 0 & p \neq q. \end{cases}
\end{aligned} \tag{4.22}$$

4.2.2 The sum of trigonometric functions

In the same way as for the Hankel function, we need to isolate the singularity in this term, and evaluate it analytically on its own, before adding it back into the rest of the expression after it is calculated numerically. The singularity occurs for the term $\langle \widehat{K}^{(2)} \chi_p, \chi_q \rangle$ when $x = x_0$ since the sum no longer converges as the n^{th} term becomes proportional to $\frac{1}{n}$ as shown below. When $x = x_0$

$$\begin{aligned}
& \int_{\text{gap}} \int_{\text{gap}} \sum_{n=0}^{\infty} \left\{ \frac{\cos[\lambda_n(x_0 + a)] \cos[\lambda_n(x_0 + a)] \cos[\alpha_n b]}{a \epsilon_n \alpha_n \sin(\alpha_n b)} \right\} \left\{ \frac{T_p(\frac{x}{g}) T_q(\frac{x_0}{g})}{\sqrt{g^2 - x^2} \sqrt{g^2 - x_0^2}} \right\} dx dx_0 \\
&= \int_{\text{gap}} \int_{\text{gap}} \sum_{n=0}^{\infty} \left\{ \frac{\cos^2[\lambda_n(x_0 + a)] \cos[\alpha_n b]}{a \epsilon_n \alpha_n \sin(\alpha_n b)} \right\} \left\{ \frac{T_p(\frac{x_0}{g}) T_q(\frac{x_0}{g})}{\sqrt{g^2 - x_0^2}} \right\} dx_0 dx_0 \\
&= \int_{\text{gap}} \int_{\text{gap}} \sum_{n=0}^{\infty} \left\{ \frac{(1 + \cos[2\lambda_n(x_0 + a)]) \cos[\alpha_n b]}{2a \epsilon_n \alpha_n \sin(\alpha_n b)} \right\} \left\{ \frac{T_p(\frac{x_0}{g}) T_q(\frac{x_0}{g})}{\sqrt{g^2 - x_0^2}} \right\} dx_0 dx_0 \\
&= \int_{\text{gap}} \int_{\text{gap}} \sum_{n=0}^{\infty} \left\{ \frac{\cos[\alpha_n b]}{2a \epsilon_n \alpha_n \sin(\alpha_n b)} + \frac{\cos[2\lambda_n(x_0 + a)] \cos[\alpha_n b]}{2a \epsilon_n \alpha_n \sin(\alpha_n b)} \right\} \left\{ \frac{T_p(\frac{x_0}{g}) T_q(\frac{x_0}{g})}{\sqrt{g^2 - x_0^2}} \right\} dx_0 dx_0
\end{aligned} \tag{4.23}$$

The first term in the integral in the one that causes the problem since for large n ,

$\alpha_n \approx i\lambda_n = \frac{in\pi}{2a}$. This means that when n is sufficiently large, then

$$\begin{aligned}
\frac{\cos[\alpha_n b]}{2a\epsilon_n \alpha_n \sin(\alpha_n b)} &\approx \frac{\cos\left[\frac{inb\pi}{2a}\right]}{in\pi \sin\left(\frac{inb\pi}{2a}\right)} \\
&= \frac{\cosh\left(\frac{nb\pi}{2a}\right)}{in\pi \sinh\left(\frac{nb\pi}{2a}\right)} \\
&= -\frac{\cosh\left(\frac{nb\pi}{2a}\right)}{n\pi \sinh\left(\frac{nb\pi}{2a}\right)} \\
&= \frac{-1}{n\pi} + o\left(\frac{1}{n}\right),
\end{aligned} \tag{4.24}$$

the sum of which does not converge. In fact, identity (4.17) shows that a log singularity forms in $K^{(2)}$ when $x = x_0$. As before, this problem can be avoided by both adding and subtracting the singularity by using the rearrangement shown in (4.25). The $n = 0$ term in the sum term is separated out, in order to make use of the identity (4.17) in further simplification.

$$\begin{aligned}
&\int_{-g}^g \int_{-g}^g \sum_{n=0}^{\infty} \left\{ \frac{\cos[\lambda_n(x_0 + a)] \cos[\lambda_n(x + a)] \cos[\alpha_n b]}{a\epsilon_n \alpha_n \sin(\alpha_n b)} \right\} \left\{ \frac{T_p\left(\frac{x}{g}\right)}{\sqrt{g^2 - x^2}} \frac{T_q\left(\frac{x_0}{g}\right)}{\sqrt{g^2 - x_0^2}} \right\} dx dx_0 \\
&= \int_{-g}^g \int_{-g}^g \left\{ \frac{\cos(kb)}{2ak\sin(kb)} + \sum_{n=1}^{\infty} \frac{\cos[\lambda_n(x_0 + a)] \cos[\lambda_n(x + a)]}{a} \left[\frac{\cos(\alpha_n b)}{\alpha_n \sin(\alpha_n b)} + \frac{2a}{n\pi} \right] \right. \\
&\quad \left. - \sum_{n=1}^{\infty} \frac{2\cos[\lambda_n(x_0 + a)] \cos[\lambda_n(x + a)]}{n\pi} \right\} \left\{ \frac{T_p\left(\frac{x}{g}\right)}{\sqrt{g^2 - x^2}} \frac{T_q\left(\frac{x_0}{g}\right)}{\sqrt{g^2 - x_0^2}} \right\} dx dx_0.
\end{aligned} \tag{4.25}$$

The first summation term now converges, and the log singularity has been isolated in the second summation term, which then needs to be integrated analytically. In order to do this the following rearrangement of this second summation term needs to be made, using equation (4.17). This process is also used by Porter [1] in his work. Then the

substitutions $x = g\cos u$ and $x_0 = g\cos v$ are made as before. Thus,

$$\begin{aligned}
& \int_{-g}^g \int_{-g}^g \frac{2}{\pi} \sum_{n=1}^{\infty} \frac{\cos[\lambda_n(x_0 + a)]\cos[\lambda_n(x + a)]}{n} \left\{ \frac{T_p(\frac{x}{g})}{\sqrt{g^2 - x^2}} \frac{T_q(\frac{x_0}{g})}{\sqrt{g^2 - x_0^2}} \right\} dx dx_0 \\
&= -\frac{1}{\pi} \int_{-g}^g \int_{-g}^g \ln \left\{ 2 \left| \cos\left[\frac{\pi}{2a}(x_0 + a)\right] - \cos\left[\frac{\pi}{2a}(x + a)\right] \right| \right\} \left\{ \frac{T_p(\frac{x}{g})}{\sqrt{g^2 - x^2}} \frac{T_q(\frac{x_0}{g})}{\sqrt{g^2 - x_0^2}} \right\} dx dx_0 \\
&= -\frac{1}{\pi} \int_0^\pi \int_0^\pi \ln \left\{ 2 \left| \cos\left[\frac{\pi}{2a}(g\cos v + a)\right] - \cos\left[\frac{\pi}{2a}(g\cos u + a)\right] \right| \right\} \cos(pu) \cos(qv) du dv \\
&= -\frac{1}{\pi} \int_0^\pi \int_0^\pi \ln \left\{ 2 \left| \sin\left[\frac{\pi}{2a}g\cos u\right] - \sin\left[\frac{\pi}{2a}g\cos v\right] \right| \right\} \cos(pu) \cos(qv) du dv \\
&= -\frac{1}{\pi} \int_0^\pi \int_0^\pi \left\{ \ln \left| \frac{\sin\left[\frac{\pi}{2a}g\cos u\right] - \sin\left[\frac{\pi}{2a}g\cos v\right]}{(\cos u - \cos v) \frac{\pi g}{2a} \cos\left(\frac{\pi g}{2a}\cos v\right)} \right| \right. \\
&\quad \left. \ln(2|\cos u - \cos v|) + \ln \left| \frac{\pi g}{2a} \cos\left(\frac{\pi g}{2a}\cos v\right) \right| \right\} \cos(pu) \cos(qv) du dv.
\end{aligned} \tag{4.26}$$

The first and third terms are smooth and can be added back into the rest of the original summation to be integrated numerically. The second term is the only part with the singularity which now needs to be integrated analytically. Again the identity (4.17) is used in order to re-write the log term as a trigonometric function that can be easily integrated and this gives

$$\begin{aligned}
& \int_0^\pi \int_0^\pi -\frac{1}{\pi} \ln(2|\cos u - \cos v|) \cos(pu) \cos(qv) du dv \\
&= -\frac{1}{\pi} \int_0^\pi \int_0^\pi -2 \sum_{n=1}^{\infty} \frac{1}{n} \cos n u \cos n v \cos p u \cos q v du dv \\
&= \frac{2}{\pi} \sum_{n=1}^{\infty} \frac{1}{n} \left[\int_0^\pi \cos n u \cos p u du \right] \left[\int_0^\pi \cos n v \cos q v dv \right] \\
&= \frac{\pi}{2p} \quad \text{for } p = q \neq 0.
\end{aligned} \tag{4.27}$$

So we have now found that

$$\begin{aligned}
& \langle \widehat{K}^{(2)} \chi_p, \chi_q \rangle \\
&= \int_0^\pi \int_0^\pi \left\{ -\frac{\cos(kb)}{2ak\sin(kb)} \right. \\
&\quad - \sum_{n=1}^{\infty} \frac{\cos[\lambda_n(g\cos v + a)]\cos[\lambda_n(g\cos u + a)]}{a} \left[\frac{\cos(\alpha_n b)}{\alpha_n \sin(\alpha_n b)} + \frac{2a}{n\pi} \right] \\
&\quad - \frac{1}{\pi} \ln \left| \frac{\sin[\frac{\pi}{2a}g\cos u] - \sin[\frac{\pi}{2a}g\cos v]}{(\cos u - \cos v)\frac{\pi g}{2a}\cos(\frac{\pi g}{2a}\cos v)} \right| - \frac{1}{\pi} \ln \left| \frac{\pi g}{2a} \cos(\frac{\pi g}{2a}\cos v) \right| \left. \right\} \cos p u \cos q v \, du \, dv \\
&\quad + \begin{cases} \frac{\pi}{2p} & p = q \neq 0 \\ 0 & \text{otherwise.} \end{cases}
\end{aligned} \tag{4.28}$$

If we now combine the expressions for $\langle \widehat{K}^{(1)} \chi_p, \chi_q \rangle$ and $\langle \widehat{K}^{(2)} \chi_p, \chi_q \rangle$, we can get the expression (4.29) for the quantity that remains to be evaluated numerically. This evaluation will be done by writing a program in Matlab, which evaluates (4.29) and then adds in the analytical solutions as detailed above in order to find $\langle \widehat{K} \chi_p, \chi_q \rangle$ for $q = 0, \dots, P$.

$$\begin{aligned}
& \int_0^\pi \int_0^\pi \left\{ \frac{i}{2} \left[H_0(kg|\cos u - \cos v|) - \frac{2i}{\pi} \ln|\cos u - \cos v| \right] \right. \\
&\quad - \frac{\cos(kb)}{2ak\sin(kb)} - \sum_{n=1}^{\infty} \frac{\cos[\lambda_n(g\cos v + a)]\cos[\lambda_n(g\cos u + a)]}{a} \left[\frac{\cos(\alpha_n b)}{\alpha_n \sin(\alpha_n b)} + \frac{2a}{n\pi} \right] \\
&\quad - \frac{1}{\pi} \ln \left| \frac{\sin[\frac{\pi}{2a}g\cos u] - \sin[\frac{\pi}{2a}g\cos v]}{(\cos u - \cos v)\frac{\pi g}{2a}\cos(\frac{\pi g}{2a}\cos v)} \right| - \frac{1}{\pi} \ln \left| \frac{\pi g}{2a} \cos(\frac{\pi g}{2a}\cos v) \right| \left. \right\} \cos p u \cos q v \, du \, dv.
\end{aligned} \tag{4.29}$$

4.3 The Asymmetric case: adapting the integral equation

Up to this point, we have assumed the gap in the harbour mouth to be centred within the harbour walls. We now consider the more general case in which the gap occupies

$x \in (-g_1, g_2)$; putting $g_1 = g_2 = g$ would return us to the simpler case already dealt with above. We now investigate in some detail how this change affects equation (4.8).

4.3.1 The right hand side of (4.8)

The test function still needs to be a Chebyshev polynomial, but this time in order to satisfy the edge condition (3.27) we will take

$$\chi_l = \frac{T_l\left(\frac{2x+g_1-g_2}{g_1+g_2}\right)}{\sqrt{(x+g_1)(g_2-x)}}. \quad (4.30)$$

The right hand side of the integral equation once the inner product has been taken (4.8), will be affected by this change, and now the substitutions that need to be used to simplify this side are $x = \frac{1}{2}(g_2 - g_1 + (g_1 + g_2) \cos u)$ and $x_0 = \frac{1}{2}(g_2 - g_1 + (g_1 + g_2) \cos v)$. The right hand side then becomes

$$\begin{aligned} (F_\beta, \chi_q) &= 2A \int_{-g_1}^{g_2} e^{-ikx \cos \beta} \frac{T_q\left(\frac{2x+g_1-g_2}{g_1+g_2}\right)}{\sqrt{(x+g_1)(g_2-x)}} dx \\ &= 2A \int_0^\pi e^{-\frac{1}{2}ik \cos \beta (g_2 - g_1 + (g_1 + g_2) \cos u)} \cos(qu) du \\ &= 2A e^{-\frac{1}{2}ik \cos(\beta)(g_2 - g_1)} \pi (-i)^q J_q\left(\frac{1}{2}k(g_1 + g_2) \cos \beta\right). \end{aligned} \quad (4.31)$$

4.3.2 The left hand side of (4.8)

Both the kernels with the Hankel term $K^{(1)}$ and the trigonometric sum term $K^{(2)}$ within equation (4.10) need to be adjusted to take account of the new gap. Firstly for the Hankel term, the inner product given in (4.12) simply needs the substitution $g = \frac{1}{2}(g_1 + g_2)$ to be made. The results for the various values of p and q that are given in (4.15) to (4.21) still hold. In the case of $u = v$, the explicit substitution made in the Matlab program to deal with the potential singularity given in (5.8) still holds, but again with the substitution $g = \frac{1}{2}(g_1 + g_2)$.

For the trigonometric sum term, several adaptations need to be made. The substitutions $x = \frac{1}{2}(g_2 - g_1 + (g_1 + g_2) \cos u)$ and $x_0 = \frac{1}{2}(g_2 - g_1 + (g_1 + g_2) \cos v)$ need to be

used when replacing x and x_0 in equation (4.25). When dealing with the singularity in this expression the following changes to the rearrangement as shown in (4.26) need to be made.

$$\begin{aligned}
& \frac{2}{\pi} \sum_{n=1}^{\infty} \frac{\cos[\lambda_n(x_0 + a)] \cos[\lambda_n(x + a)]}{n} \\
&= -\frac{1}{\pi} \ln \left\{ 2 \left| \sin\left[\frac{\pi}{4a}(g_2 - g_1 + (g_1 + g_2) \cos u)\right] - \sin\left[\frac{\pi}{4a}(g_2 - g_1 + (g_1 + g_2) \cos v)\right] \right| \right\} \\
&= -\frac{1}{\pi} \ln \left| \frac{\sin\left[\frac{\pi}{4a}(g_2 - g_1 + (g_1 + g_2) \cos u)\right] - \sin\left[\frac{\pi}{4a}(g_2 - g_1 + (g_1 + g_2) \cos v)\right]}{(\cos u - \cos v) \frac{\pi}{4a}(g_1 + g_2) \cos\left[\frac{\pi}{4a}(g_2 - g_1 + (g_1 + g_2) \cos v)\right]} \right| \\
&\quad - \frac{1}{\pi} \ln[2|\cos u - \cos v|] - \frac{1}{\pi} \left| \frac{\pi}{4a}(g_1 + g_2) \cos\left[\frac{\pi}{4a}(g_2 - g_1 + (g_1 + g_2) \cos v)\right] \right|.
\end{aligned} \tag{4.32}$$

The analytical solution in (4.27) still applies, and the limit of the first log term still tends to one for the same reason as that shown in (5.11).

These adaptations need to be substituted into the Matlab program, which can then of course be run for both symmetric and asymmetric cases.

Chapter 5

Programming a solution method

In this chapter we shall look at the method used to program a solution to the integral equation (3.34) using Matlab. In particular, we shall look at the adjustments that need to be made to take account of the log singularities in the integral equation, and how the program can be tested to check for convergence in the solution.

5.1 Programming the Galerkin method

Having taken the original integral equation

$$(\widehat{K}v_\beta)(x) = F_\beta(x) \quad (5.1)$$

and found expressions for the components of the weak form

$$\sum_{p=0}^P \langle \widehat{K}\chi_p, \chi_q \rangle t_p = \langle F_\beta, \chi_q \rangle \quad \text{for } q = 0, 1, \dots, P. \quad (5.2)$$

this system of simultaneous equations can be written as a matrix equation of the form

$$\kappa \mathbf{t} = \widetilde{\mathbf{F}} \quad (5.3)$$

where

$$\kappa = \begin{pmatrix} \langle \widehat{K}_{\chi_0, \chi_0} \rangle & \langle \widehat{K}_{\chi_1, \chi_0} \rangle & \dots & \dots & \dots & \langle \widehat{K}_{\chi_P, \chi_0} \rangle \\ \langle \widehat{K}_{\chi_0, \chi_1} \rangle & \langle \widehat{K}_{\chi_1, \chi_1} \rangle & \dots & \dots & \dots & \langle \widehat{K}_{\chi_P, \chi_1} \rangle \\ \vdots & \vdots & & & & \vdots \\ \vdots & \vdots & & & & \vdots \\ \vdots & \vdots & & & & \vdots \\ \langle \widehat{K}_{\chi_0, \chi_P} \rangle & \langle \widehat{K}_{\chi_1, \chi_P} \rangle & \dots & \dots & \dots & \langle \widehat{K}_{\chi_P, \chi_P} \rangle \end{pmatrix} \quad (5.4)$$

and

$$\tilde{\mathbf{F}} = \begin{pmatrix} \langle F_\beta, \chi_0 \rangle \\ \langle F_\beta, \chi_1 \rangle \\ \vdots \\ \vdots \\ \vdots \\ \langle F_\beta, \chi_P \rangle \end{pmatrix} \quad (5.5)$$

This matrix equation is then solved in Matlab, using the in-built Gaussian elimination function. The matrix entries $\langle \widehat{K}_{\chi_p, \chi_q} \rangle$ are found using the Matlab function “dblquad” which numerically evaluates a double integral. Once \mathbf{t} is found, $v_\beta(x_0)$ can be constructed, and then the solution for inside the harbour, ϕ_d^- , and outside the harbour, $\phi^+ = \phi_d^+ + \phi_i + \phi_r$, can be plotted.

5.2 Singularities

Although the log singularities have been removed and dealt with analytically (and are then added back into the solution within the program), there are three terms within the integral (4.29) that are to be evaluated where the program will still react poorly to the apparent appearance of a singularity. Therefore in these cases where $u = v$, the terms need to be simplified and explicitly stated within the program to avoid problems.

For the Hankel function term, the problem is caused when $u = v$ in

$$\int_0^\pi \int_0^\pi \frac{i}{2} \left[H_0^{(1)}(kg|\cos u - \cos v|) - \frac{2i}{\pi} \ln|\cos u - \cos v| \right] \cos pu \cos qv \, du \, dv \quad (5.6)$$

where the program will try to evaluate $\ln(0)$. In order to avoid this the following approximation is used and substituted explicitly into the program when $|u - v|$ is very small. The asymptotic forms of the Bessel functions for small arguments are

$$\begin{aligned} Y_0(z) &\approx \frac{2}{\pi} \left[\ln\left(\frac{z}{2}\right) + \gamma \right] \\ J_0(z) &\approx \frac{1}{\Gamma(1)} = 0! = 1 \end{aligned} \quad (5.7)$$

where Γ is the gamma function $\Gamma(n) = (n - 1)!$ where $n \in \mathbb{N}$ and $\gamma = 0.57721566$ (to 8 decimal places) is the Euler-Mascheroni constant (see Wolfram Mathworld [6]). Therefore the problem term can be re-written as follows for small $|u - v|$:

$$\begin{aligned} H_0^{(1)}(kg|\cos u - \cos v|) - \frac{2i}{\pi} \ln|\cos u - \cos v| \\ = 1 + \frac{2i}{\pi} \left\{ \ln\left[\frac{kg|\cos u - \cos v|}{2}\right] + \gamma \right\} - \frac{2i}{\pi} \ln|\cos u - \cos v| \\ = 1 + \frac{2i}{\pi} \left[\ln\left(\frac{kg}{2}\right) + \gamma \right]. \end{aligned} \quad (5.8)$$

In the case of the terms produced by the original trigonometric sum term, the only problem occurs in the following log term when $u = v$:

$$\int_0^\pi \int_0^\pi -\frac{1}{\pi} \ln \left| \frac{\sin\left[\frac{\pi}{2a}g\cos u\right] - \sin\left[\frac{\pi}{2a}g\cos v\right]}{(\cos u - \cos v)\frac{\pi g}{2a} \cos\left(\frac{\pi g}{2a}\cos v\right)} \right| \cos pu \cos qv \, du \, dv. \quad (5.9)$$

Again, the program will try and evaluate $\ln(0)$ unless instructed otherwise. However we can apply L'Hôpital's rule, since

$$\begin{aligned} \lim_{u \rightarrow v} \sin\left[\frac{\pi}{2a}g\cos u\right] - \sin\left[\frac{\pi}{2a}g\cos v\right] \\ = \lim_{u \rightarrow v} (\cos u - \cos v) \frac{\pi g}{2a} \cos\left(\frac{\pi g}{2a}\cos v\right) = 0 \end{aligned} \quad (5.10)$$

and therefore work out the limit as u approaches v manually. In fact it can be found that the limit of the argument of the log term is

$$\begin{aligned} \lim_{u \rightarrow v} \frac{\sin[\frac{\pi}{2a}g\cos u] - \sin[\frac{\pi}{2a}g\cos v]}{(\cos u - \cos v)^{\frac{\pi g}{2a}} \cos(\frac{\pi g}{2a}\cos v)} \\ = \lim_{u \rightarrow v} \frac{\frac{d}{du}(\sin[\frac{\pi}{2a}g\cos u] - \sin[\frac{\pi}{2a}g\cos v])}{\frac{d}{du}((\cos u - \cos v)^{\frac{\pi g}{2a}} \cos(\frac{\pi g}{2a}\cos v))} = 1. \end{aligned} \quad (5.11)$$

This can now be substituted in for the cases where $|u - v|$ is small.

5.3 Checks for convergence

In order to check that the results seem accurate, the amplitude of the diffracted waves in the far field can be analysed. This can be done by using the approximation to the diffracted wave outside the harbour. This is found by using the asymptotic forms of the Bessel functions for large arguments (see Wolfram Mathworld [6])

$$\begin{aligned} J_0(z) &= \sqrt{\frac{2}{\pi z}} \cos(z - \frac{\pi}{4}) \\ Y_0(x) &= \sqrt{\frac{2}{\pi x}} \sin(x - \frac{\pi}{4}) \end{aligned} \quad (5.12)$$

to obtain

$$\begin{aligned} \phi_d^+(x, y) &= -\frac{i}{2} \int_{-g}^g v_\beta(x_0) H_0^{(1)}\{k\sqrt{(x-x_0)^2 + y^2}\} dx_0 \\ &\approx -\frac{i}{2} \int_{-g}^g v_\beta(x_0) \left[\frac{2e^{i(k\sqrt{(x-x_0)^2 + y^2} - \frac{\pi}{4})}}{\sqrt{2\pi k\sqrt{(x-x_0)^2 + y^2}}} \right] dx_0. \end{aligned} \quad (5.13)$$

If we now let $x = r \cos \psi$ and $y = r \sin \psi$ where $x^2 + y^2 = r^2$ and ψ is the angle between

a point (x, y) in the far-field and the coastal wall, then for large x, y

$$\phi_d^+(x, y) \approx -\frac{i}{2} \int_{-g}^g v_\beta(x_0) \left[\frac{2e^{i(kr\sqrt{1-\frac{2}{r}x_0\cos\psi+\frac{x_0^2}{r^2}-\frac{\pi}{4}})}}{\sqrt{2\pi kr}} \right] dx_0. \quad (5.14)$$

We can then apply the Binomial expansion, since for large r , $\frac{2}{r}\cos\psi$ is small, and $(\frac{x_0}{r})^2 \rightarrow 0$ giving

$$\begin{aligned} \phi_d^+(x, y) &\approx -\frac{i}{2} \int_{-g}^g v_\beta(x_0) \left[\frac{2e^{i(kr[1-\frac{1}{r}x_0\cos\psi]-\frac{\pi}{4})}}{\sqrt{2\pi kr}} \right] dx_0 \\ &\approx \int_{-g}^g v_\beta(x_0) \left[\frac{e^{ikr}e^{-ikx_0\cos\psi}(-ie^{-i\frac{\pi}{4}})}{\sqrt{2\pi kr}} \right] dx_0 \\ &\approx \frac{Ae^{i(kr-\frac{3\pi}{4})}}{(2\pi kr)^{\frac{1}{2}}} G(\psi, \beta) \end{aligned} \quad (5.15)$$

where $G(\psi, \beta) = \frac{1}{A} \int_{-g}^g v_\beta(x_0)e^{-ikx_0\cos\psi} dx_0$ is the diffraction coefficient.

5.3.1 The breakwater problem

If the term $K^{(2)}$ is temporarily deleted from the kernel K in equation (3.34), then the solution $v_\beta(x_0)$ solves the corresponding thin breakwater problem, a special case ($d = 0$) of that described in section 2.2, and results can be compared with those of Linton & McIver [2]. This process allows the accuracy of a large section of the Matlab code to be verified. In the following tables, results for various values of P and k are compared, using $\psi = \frac{11\pi}{12}$ and $\beta = \frac{\pi}{12}$.

	P				
kg	5	10	15	20	25
π	3.9961	3.9966	3.9966	3.9966	3.9966
2π	5.2115	5.7156	5.7156	5.7156	5.7156
3π	3.5247	7.1161	7.1336	7.1336	7.1336
4π	2.8843	7.3812	8.4462	8.4468	8.4468

Table 5.1: Results for the breakwater problem.

In these results, for each of the different wave frequencies it is clear that the scheme is achieving convergence as P is increased. As k increases the convergence is at a slower rate due to more rapid variation in the derivative function $v_\beta(x_0)$. My results and those of Linton & McIver are very close. The slight differences, especially for small P are probably due to a different numerical computation scheme being used to calculate the integrals (it is not specified in the work). The almost identical convergence values suggest that my scheme is at least accurate for the Hankel part of the kernel.

	P				
kg	5	10	15	20	25
π	3.9883	3.9966	3.9966	3.9966	3.9966
2π	3.6659	5.7155	5.7156	5.7156	5.7156
3π	3.4499	7.0447	7.1336	7.1336	7.1336
4π	3.0742	5.6521	8.4435	8.4468	8.4468

Table 5.2: Linton & McIver's results with the Galerkin method.

5.3.2 The full harbour problem

If $v_\beta(x_0)$ is now worked out for the full integral equation (3.30) for the harbour problem, then convergence can be analysed both for the number of terms, P , required in the Galerkin method, and also the number of terms, J , required for the trigonometric sum term. In the following tables P is kept constant while J is analysed, and vice versa.

Convergence is clearly indicated by the values in Tables 5.3 and 5.4, even for relatively small values of J and P . In fact the Galerkin method has immediately converged for $k \leq 6$ even when taking only six terms in the sum. As the wave number k increases in value, it is necessary to take more terms in the Galerkin method, but taking $P = 10$ is sufficient for full convergence up to $k = 14$.

For the trigonometric sum term, again there is immediate convergence taking only twenty terms when $k \leq 4$, and even for a k value as high as fourteen, convergence

P			
k	5	10	15
2	1.7917	1.7917	1.7917
4	2.2201	2.2201	2.2201
6	2.0673	2.0673	2.0673
8	3.0741	3.0805	3.0805
10	0.6474	0.6469	0.6469
12	3.5088	3.6906	3.6906
14	1.4038	1.7694	1.7694
16	2.2603	2.9638	2.9645
18	2.2854	4.5660	4.5786

Table 5.3: Checking for convergence with the Galerkin method for varying values of P , keeping $J = 80$.

has occurred by $J = 60$. The Matlab program needs to be run with values of P and J that ensure both sufficient accuracy, but also time efficiency. In particular, increasing P significantly lengthens the time taken to run a program to solve the integral equation, so the minimum value that can be justified needs to be used.

J				
k	20	40	60	80
2	1.7917	1.7917	1.7917	1.7917
4	2.2201	2.2201	2.2201	2.2201
6	2.0672	2.0673	2.0673	2.0673
8	3.0813	3.0806	3.0805	3.0805
10	0.6472	0.6469	0.6469	0.6469
12	3.6914	3.6907	3.6906	3.6906
14	1.7693	1.7694	1.7694	1.7694
16	2.9684	2.9643	2.9639	2.9638
18	4.5698	4.5664	4.5660	4.5660

Table 5.4: Checking for convergence in the sum term for varying values of J , keeping $P = 10$.

Chapter 6

Results

6.1 Interpretation of the graph plots

In the following graph plots of the harbour and the external area, a shaded contour plot has been used. The contours represent the heights of the waves at time $t = 0$, and the key for the contour colours is shown next to each plot as in Figure 6.1 below. The scale varies for different plots, but the red areas always indicate peaks, and the blue areas troughs.

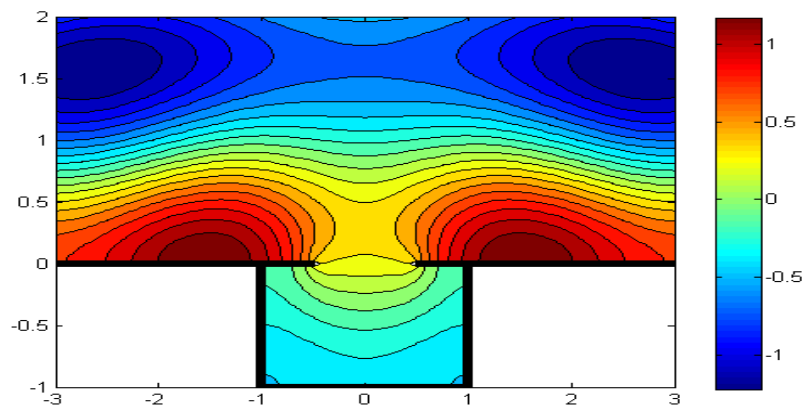


Figure 6.1: Exemplar plot.

For all results in this and following chapters, the plane wave amplitude A has been set

to 0.5. The greatest wave height outside the harbour therefore generally approaches a maximum of 1m, indicating points where reflected and incident waves of height 0.5m combine.

The elevation above the undisturbed free surface is given by

$$\eta(x, y, t) = \text{Re}[\phi(x, y)e^{-i\sigma t}] \quad (6.1)$$

where t represents time and σ is dependent upon the wave number k as defined in (2.2). For $t = 0$, the real part of the solution $\phi(x, y)$ needs to be plotted in order to represent the heights of the waves, and all the graphs in this chapter are created by plotting this.

6.2 Continuity over the gap

Before assessing any outcomes from the graph plots of the harbour and its exterior, it is important to check that the solution plotted inside and outside the harbour is matching over the gap. In Figures 6.2 to 6.4 the case where $k = 1$ and $\beta = \frac{\pi}{4}$ is looked at in detail. In these results, the harbour has been defined with $a = b = 1$, i.e. width 2 and length 1, and the harbour walls extend in with $g = 0.5$. In Figure 6.2 the harbour mouth is magnified so the contour lines can be visually analysed. There is no obvious discrepancy even at a fairly high level of magnification.

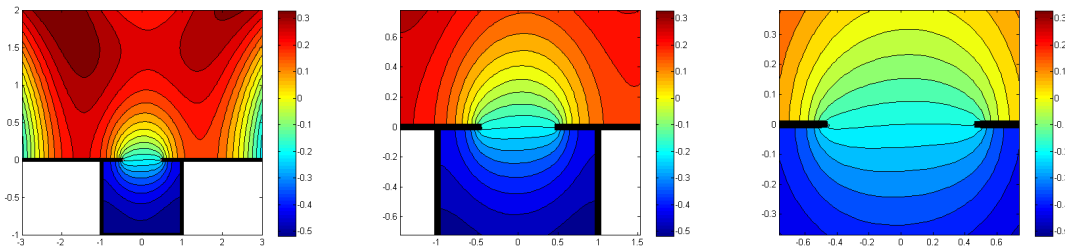


Figure 6.2: Incident wave at an angle $\beta = \pi/4$, and frequency $k = 1$, zooming in on the gap.

In Figure 6.3 several slices are taken parallel to the y axis for both the real and imaginary parts of the solution. Any discrepancies would be easy to spot on these, but they show the solution inside and outside the harbour to be continuous, and furthermore the

derivatives of the functions for these solutions are continuous over the harbour mouth (at $y = 0$).

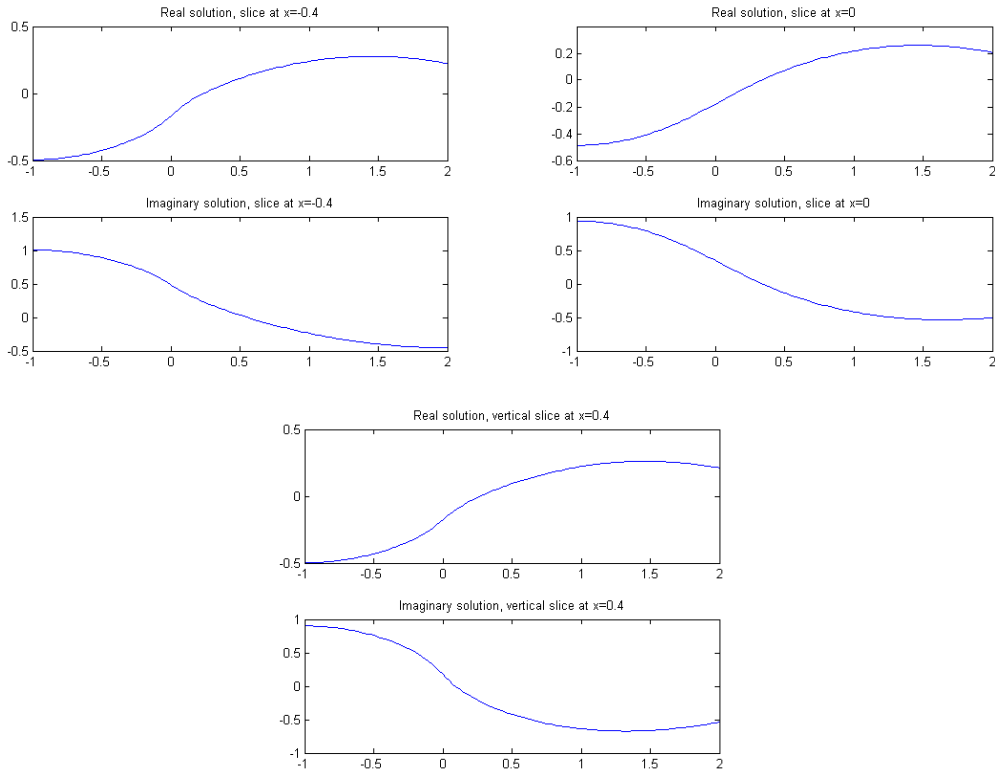


Figure 6.3: Slices parallel to the y axis checking for continuity over the gap for $k = 1$ and $\beta = \pi/4$, with $x = -0.4, 0$ and 0.4 respectively.

In 6.4 a slice parallel to the x axis is taken fractionally above and below the gap for both the real and imaginary parts of the solution. The solution in the harbour is shown in green, the solution outside the harbour is in red and the solution across the gap is in blue. It can be seen that these match up extremely closely through the gap itself.

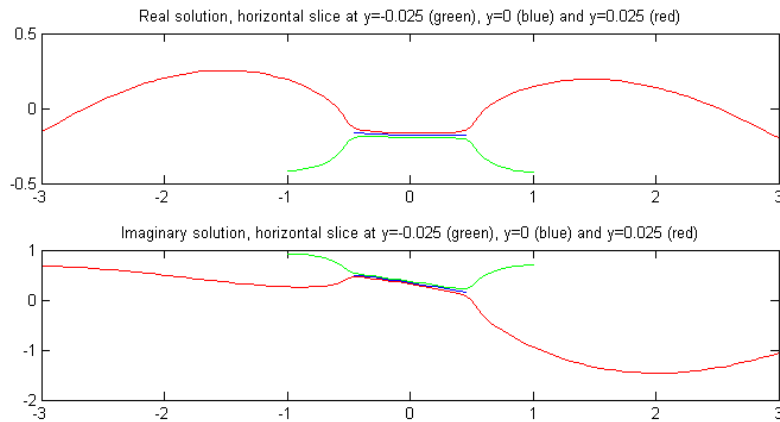


Figure 6.4: Slice parallel to the x axis checking for continuity over the gap for $k = 1$ and $\beta = \pi/4$.

6.3 The effect of changing k , β and g

In this section we analyse the effect of varying the values of the wave number k , the angle of the incident wave β and the size of the gap g on the behaviour of the waves within the harbour.

6.3.1 Altering k and β

The following Figures 6.5 to 6.9 contain contour plots for values of k ranging from 1 to 4 respectively, and each figure has a different angle β ranging from $\pi/2$ to $\pi/6$. The basic effects of altering either k and β can therefore be seen and will be analysed for the harbour. In these plots, the harbour has been defined with $a = b = 1$, and the harbour walls extend in with $g = 0.5$. Since the wave amplitude is set at $A = 0.5$, the wave heights range from approximately minus one to plus one in height. In the following accounts, I will describe waves that are approaching 1m in height as being of ‘maximum’ height, waves that are at roughly at the height of the undisturbed free surface as being of ‘medium’ height, and waves that are close to -1m in height as being ‘low’.

Looking at the effect of changing k first, as k increases the amplitude of the waves always increases. There is some variation as to whether this is achieved through an increase in solely maximum height or minimum height, or in some cases changes to both. When $k = 1$ the waves in the harbour are always low regardless of angle of incidence. At

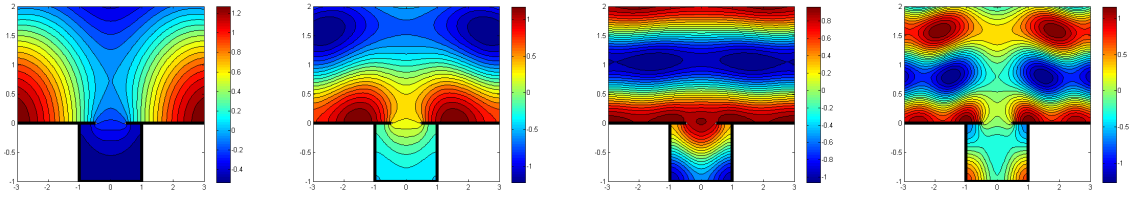


Figure 6.5: Incident wave at an angle $\beta = \pi/2$, and wave numbers $k = 1, 2, 3$ and 4 respectively.

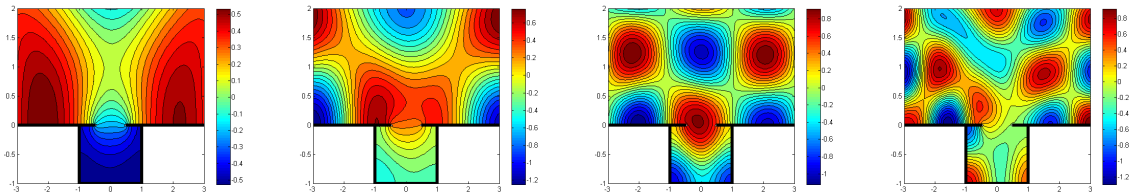


Figure 6.6: Incident wave at an angle $\beta = \pi/3$, and wave numbers $k = 1, 2, 3$ and 4 respectively.

$k = 2$ the waves are still fairly low in the majority of the harbour, but achieve a medium range height in the gap. By $k = 3$ the waves generally range from being very low in the back two corners of the harbour, of medium height throughout most of the rest of the harbour, and increasing to the maximum height in the gap. For $k = 4$ the reverse situation appears, with the maximum wave height occurring in the back (unsheltered) corner(s) and the low wave heights occurring in the front corners. The middle sections and gap are then of a medium height.

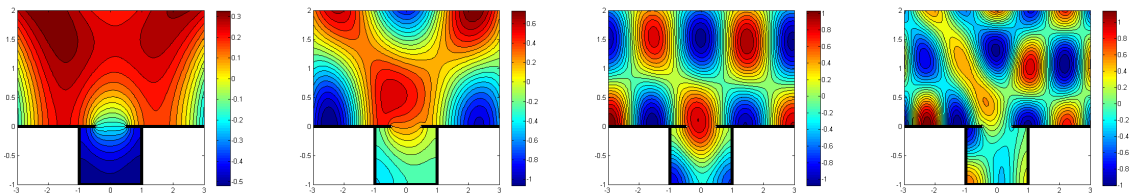


Figure 6.7: Incident wave at an angle $\beta = \pi/4$, and wave numbers $k = 1, 2, 3$ and 4 respectively.

The angle of incidence of the incoming plane wave also has some effect on the wave pattern in the harbour. For the case of $\beta = \pi/2$ there is symmetry, since the gap itself has been set up to be symmetrical in this case. As the angle increases, one side of the

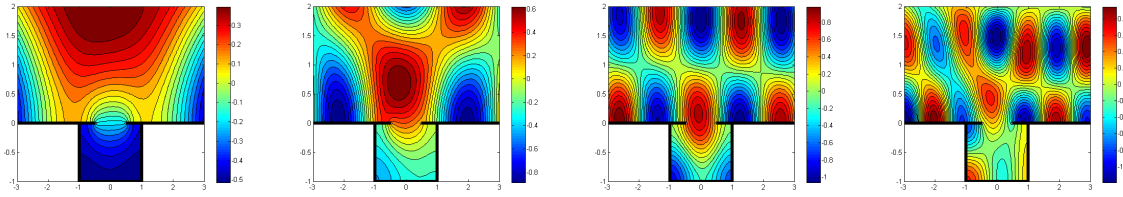


Figure 6.8: Incident wave at an angle $\beta = \pi/5$, and wave numbers $k = 1, 2, 3$ and 4 respectively.

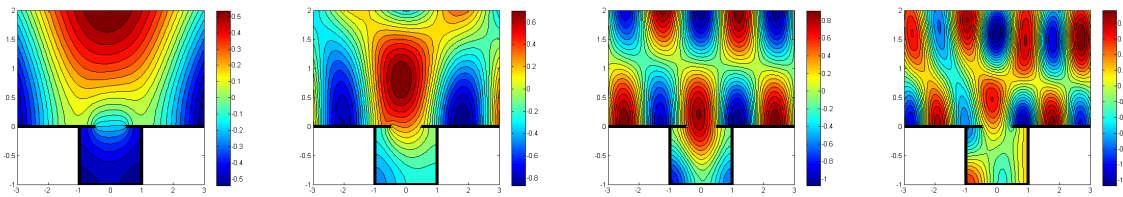


Figure 6.9: Incident wave at an angle $\beta = \pi/6$, and wave numbers $k = 1, 2, 3$ and 4 respectively.

harbour becomes sheltered from the incoming wave, and both the high and low waves are reduced in this area. On the non-sheltered side of the harbour, the change in β has very little effect on the wave heights.

6.3.2 Altering g

For the case where $\beta = \frac{\pi}{2}$, the length to which the harbour walls extend across the harbour mouth only makes a limited difference. The symmetry in this particular case means that the only real impact, as seen in Figure 6.10, is to increase the height of waves outside the harbour in a vertical channel as water is reflected back out of the harbour, and to slightly decrease the height of waves at the back of the harbour itself.

However when the symmetry is removed as in the case where $\beta = \frac{\pi}{3}$ in Figure 6.11, the effect is much more dramatic. When the harbour is almost closed, there is very little activity within the harbour, with the waves all at a medium height. Outside the harbour there is symmetry in the incident and reflected waves, showing a lack of diffracted wave from the harbour. As the gap is increased, the asymmetry grows both within and outside the harbour. By the point at which there is practically no harbour

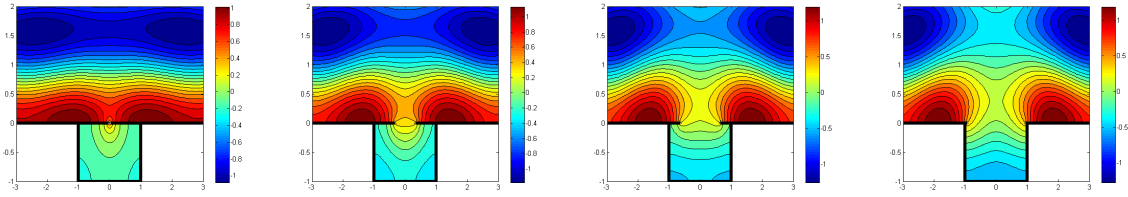


Figure 6.10: Incident wave at an angle $\beta = \pi/2$, wave number $k = 2$ and with $g=0.05, 0.35, 0.65$ and 0.95 respectively.

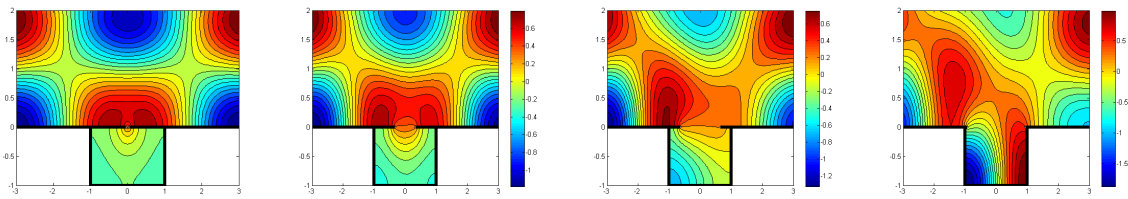


Figure 6.11: Incident wave at an angle $\beta = \pi/3$, wave number $k = 2$ and with $g=0.05, 0.35, 0.65$ and 0.95 respectively.

wall affording any protection, a significant swell can be seen within the harbour, with the right hand side having waves of maximum height, and a steep decrease in height to very low waves on the left hand side.

Chapter 7

Resonance

In this chapter we will look at finding values of k and β that will create a resonant response within the harbour. In order to start tracking possible resonant frequencies for the harbour, we can look at the resonant frequencies for a closed rectangular box. For small g , that is for a very small gap in the harbour wall, we hypothesise that any resonant frequencies will be very similar to those of the closed box problem.

7.1 Finding a suitable value of k

For a closed rectangular box, with the same dimensions as the harbour (width $2a$, length b), an eigenfunction that will set up a resonant response will be

$$\phi = F_{CD} \cos \left[\frac{C\pi}{b}(y + b) \right] \cos \left[\frac{D\pi}{2a}(x + a) \right] \quad (7.1)$$

for some integers C and D . Comparing this to our expression for the solution within the harbour (3.15) we have an eigenfunction of the form

$$\phi_a^{D-} = f_D \cos[\alpha_D(y + b)] \cos \left[\frac{D\pi}{2a}(x + a) \right] \quad (7.2)$$

where $\alpha_D = \sqrt{[k^2 - (\frac{D\pi}{2a})^2]}$. But in order to match the required format for resonance in the closed box, we need C such that $\alpha_D = \frac{C\pi}{b}$ and therefore the value for k that satisfies

this is

$$k^2 = \left(\frac{C\pi}{b}\right)^2 + \left(\frac{D\pi}{2a}\right)^2. \quad (7.3)$$

It should be noted that for this definition of k , the special case where $\alpha_n b$ may equal an integer multiple of π as described in Section 3.5 will occur. The Matlab program must therefore be written to take account of this, and follow the adjusted procedure for solution.

7.2 Maximising the effect of β

It may be possible to force an even greater response in the harbour with a careful selection of the angle β which both the incident and reflected waves are dependent upon. The expression for the plane waves (3.1) and (3.2) at the harbour mouth can be written as follows:

$$2Ae^{-ikx \cos \beta} = 2A[\cos(kx \cos \beta) - i \sin(kx \cos \beta)]. \quad (7.4)$$

Comparing this to the eigenfunction for the closed box that we are using as our model for resonance, at $y = 0$ we have

$$\begin{aligned} \phi|_{y=0} &= F_{CD} \cos[C\pi] \cos\left[\frac{D\pi}{2a}(x+a)\right] \\ &= F_{CD}(-1)^C \left[\cos\left(\frac{D\pi x}{2a}\right) \cos\left(\frac{D\pi}{2}\right) - \sin\left(\frac{D\pi x}{2a}\right) \sin\left(\frac{D\pi}{2}\right) \right]. \end{aligned} \quad (7.5)$$

We therefore expect taking $k \cos \beta = \frac{D\pi}{2a}$ to maximise any resonance within the harbour, and will test this when looking at results. Taking the value of k that we have previously

worked out, and combining it with this condition on β gives us

$$\begin{aligned}
\sqrt{\left(\frac{C\pi}{b}\right)^2 + \left(\frac{D\pi}{2a}\right)^2} \cos \beta &= \frac{D\pi}{2a} \\
\Rightarrow \left[\left(\frac{C}{b}\right)^2 + \left(\frac{D}{2a}\right)^2\right] \cos^2 \beta &= \left(\frac{D}{2a}\right)^2 \\
\Rightarrow \left(\frac{C}{b}\right)^2 \cos^2 \beta &= \left(\frac{D}{2a}\right)^2 \sin^2 \beta \\
\Rightarrow \tan \beta &= \pm \frac{2Ca}{Db}.
\end{aligned} \tag{7.6}$$

7.3 Results

As in Chapter 6 the incident wave amplitude A is set to 0.5 in all the following plots. As also detailed in Chapter 6 the elevation above the undisturbed free surface $\eta(x, y, t)$ is given by $\eta(x, y, t) = \text{Re}[\phi(x, y)e^{-i\sigma t}]$. Whereas before, we simply set $t = 0$ and therefore plotted the real part of the solution $\phi(x, y)$ to represent the heights of the waves, when searching for resonant cases we need to consider other scenarios. For cases where $-\sigma t$ is equal to odd multiples of $\frac{\pi}{2}$, we get

$$\begin{aligned}
\eta(x, y, t) &= \text{Re}[\phi(x, y)e^{-i\sigma t}] \\
&= \text{Re}[i\phi(x, y)] \\
&= \text{Im}[\phi(x, y)].
\end{aligned} \tag{7.7}$$

We therefore need to examine both the real and imaginary parts of the solution $\phi(x, y)$ for various values of k , when searching for a resonant case.

7.3.1 A resonant case in the harbour

There are two main indicators of resonance that can be seen in a contour plot of the wave heights inside and outside the harbour. Firstly the comparative heights of the waves. In the plots of non-resonant cases in Section 6.3, the maximum wave height outside the harbour was always more than or equal to the maximum height within the harbour. However where resonance occurs, the converse is true, and the maximum height should

appear within the harbour.

The other indicator of resonance relates to the pattern of the wave heights that appears within the harbour. For the non-resonant cases in Section 6.3 the maximum wave heights are all focused at one point in the harbour. In contrast, where resonance occurs, an alternating pattern of minimum and maximum wave heights appears. This can be seen in Figures 7.1 to 7.3 below.

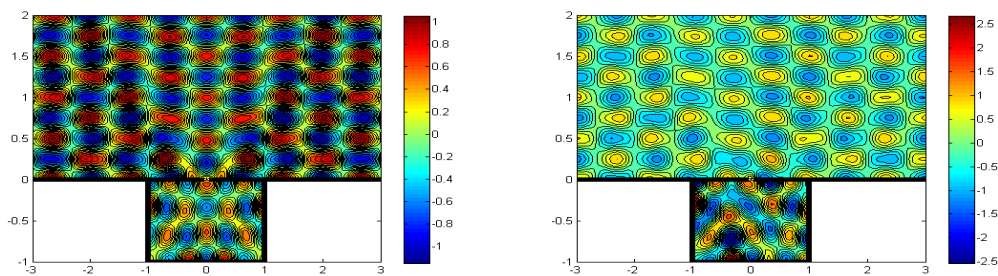


Figure 7.1: Plots of the real and imaginary solution respectively with $C = 4$ and $D = 3$.

In all the following plots in this chapter, $\tan \beta = \pm \frac{2Ca}{Db}$, $a = b = 1$ and $g = 0.05$ unless otherwise stated. If we look at plots of the real and imaginary parts of the wave heights for the case $C = 4, D = 3$ (Figure 7.1) the maximum amplitude is significantly different in the real and the imaginary case. For the real case, the maximum and minimum heights are 1 and -1 respectively both within and outside of the harbour. However where the imaginary part of the wave height is plotted, there is a significant difference in the amplitude of the waves within and outside of the harbour. Inside the harbour there is clear evidence of a resonant response, with wave heights varying from -2.5 to +2.5, whereas outside of the harbour the range is still -1 to +1. The difference in wave heights therefore satisfies our first indicator for resonance in the imaginary case, and in both the real and imaginary case the alternating pattern of minimum and maximum wave heights appears.

In Figures 7.2 and 7.3 the graphs are plots of the imaginary part of the solution $\phi(x, y)$ and they demonstrate the two different indications of a resonant effect. In Figure 7.2 they are plotted using a constant value of $C = 1$ and increasing D . In these plots

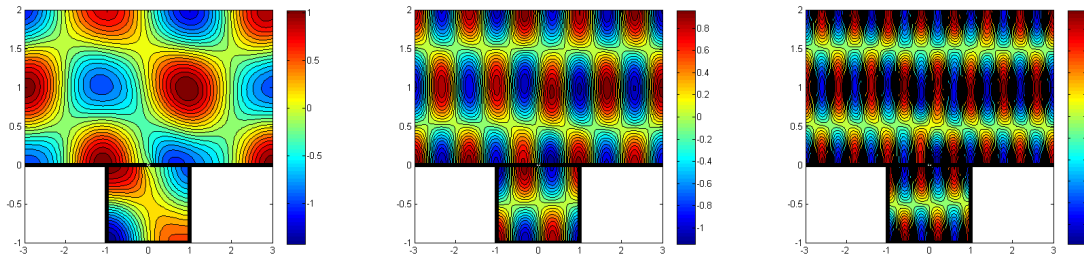


Figure 7.2: Plots of $\text{Im}(\phi)$ showing resonant response in the harbour, with $C = 1$ and $D = 1, 3, 5$ respectively.

the wave heights are the same within and outside of the harbour, but the alternating pattern of low and high waves within the harbour can be seen. It is also clear that as k increases, so does the frequency of this pattern. Moreover, this can be linked to the values of C and D , due to their contribution to the eigenfunction (7.1). C determines the number of changes from maximum to minimum height in the y direction, whereas D determines the same in the x direction.

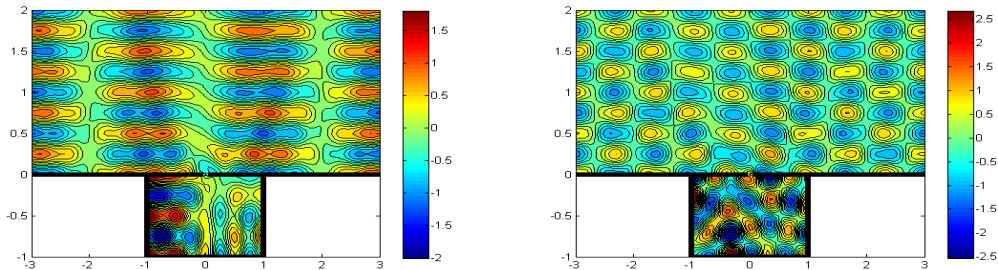


Figure 7.3: Plots of $\text{Im}(\phi)$ showing resonant response in the harbour, with $C = 4$ and $D = 1, 3$ respectively.

In Figure 7.3 the alternating pattern is less clear, but the resonance is obvious in the larger wave heights that are occurring within the harbour compared to those outside the harbour.

7.3.2 The effect of varying C and D

The real and imaginary parts of the maximum heights within the harbour are plotted in Figures 7.4 and 7.5 below. In both plots the key features appear to be linked to whether the value of D is odd or even.

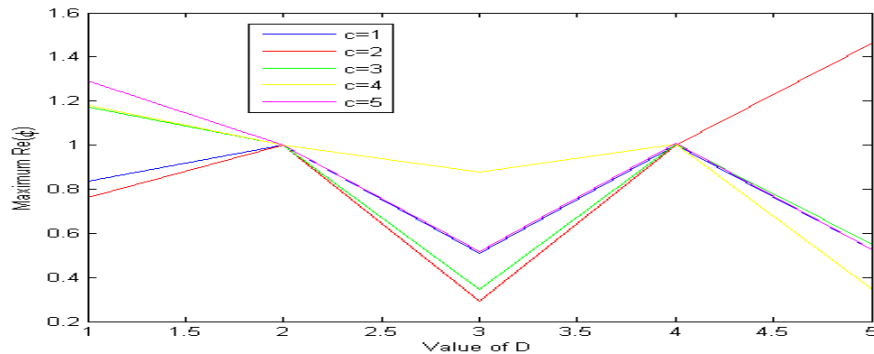


Figure 7.4: Plots of the maximum value of $\text{Re}(\phi)$ within the harbour for $g = 0.05$ and $g = 0.1$, as C and D vary.

It is clear from Figure 7.4 that for these values of C and D the real part of the wave height does not contribute significantly to the resonant effect, since the maximum heights are always less than 1.5 for this range of k . However a pattern does emerge from this plot. When D is even, the maximum real wave height is constant at a value of 1 regardless of variation in C . However when D is odd, then changing C does have an impact, although not in a way that is obviously predictable from looking at this graph.

In Figure 7.5 where the maximum imaginary part of the wave heights within the harbour is plotted, the full resonant effect of potentially high waves can be seen. Whereas for this range of k , the real part of the maximum wave height barely reaches 1.5, there are a number of cases for the imaginary part where 1.5 is exceeded, and even 3 is achieved. Interestingly again it is for odd values of D that higher waves start occurring, whereas for the even values there is no contribution towards resonance regardless of the values of C . The case where $C = 4$ and $D = 3$ in particular stands out as causing a genuinely resonant response, with exceptionally large wave heights.

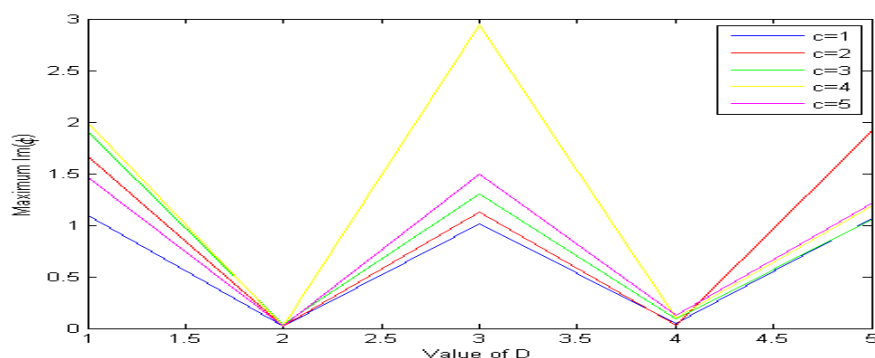


Figure 7.5: Plot of the maximum value of $\text{Im}(\phi)$ within the harbour for $g = 0.05$ and $g = 0.1$, as C and D vary.

7.3.3 The effect of β on resonance

We have hypothesised that any resonant response can be excited further by an appropriate selection of the incident wave angle, and this now needs to be verified. In Figure 7.6 the resonant case that has been discovered for $C = 4$, $D = 3$ will be looked at again, this time varying the angle β . Following the work in Section 7.2, we are expecting the largest response for $\tan \beta = \frac{2Ca}{Db} = \frac{8}{3}$.

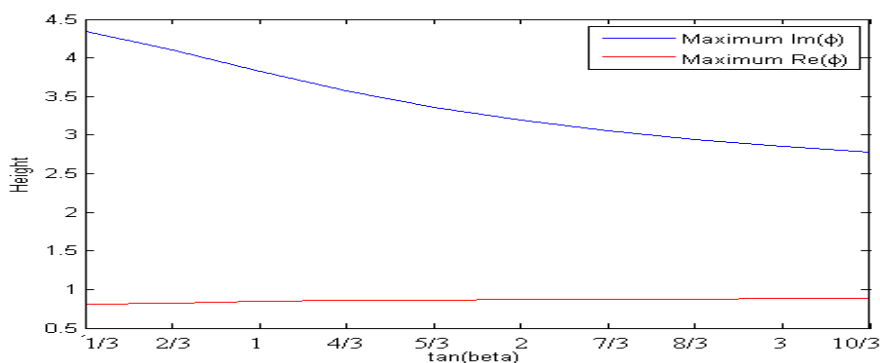


Figure 7.6: Plot of the effect of varying β on maximum wave heights

However the results in Figure 7.6 do not support this and indicate that, for these values of C , D and g , the smaller the incident angle, the larger the response from $\text{Im}(\phi)$ within the harbour. This result suggests that any resonance that the incident wave can excite is

relatively small in comparison with the effect produced by changes in the wave number k . It is likely that the reason a small angle produces the most resonance is because as the angle reduces, the area within the harbour that the incident wave has any impact on is reduced. Therefore the open harbour becomes more like the closed box case (which the resonant eigenfunctions are based upon).

7.3.4 The size of the harbour

In order to test the possible effects of altering the ratio of width to length in the harbour, the length is kept constant at $b = 1$ and the resonant case for $C = 4, D = 3$ is then plotted in Figure 7.7 with β kept constant at a value of $\tan^{-1}(\frac{8}{3})$. The width $2a$ of the harbour is varied taking values of a from 0.2 to 1 in the first graph, then 1 to 5 in the second.

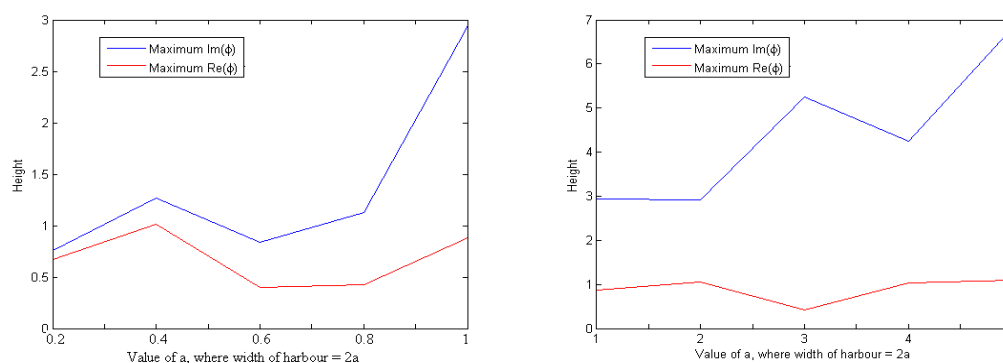


Figure 7.7: Plot of the effect of varying the harbour width on maximum wave heights

It is clear to see from the plot of $\text{Im}(\phi)$ that as the ratio of width to length increases, so does the size of the resonance. However this increase is dependent on whether a is odd or even - with odd values producing higher maximum wave heights than their consecutive even values. This is unsurprising given the odd and even pattern that has already been mentioned for D , since a and D are linked in the governing eigenfunction (7.1).

7.3.5 Changing the gap in the harbour mouth

Another factor that might be expected to affect any resonant response in the harbour, is the size of the gap in the harbour mouth. In Figure 7.8, the resonant case for $C = 4, D = 3$ is plotted with β kept constant at a value of $\tan^{-1}(\frac{8}{3})$ whilst g is varied. As expected, looking at the results for $\text{Im}(\phi)$, the resonant effect reduces as the size of the gap is increased, therefore making the harbour less like the closed box scenario, and so making the choice of eigenfunctions less appropriate.

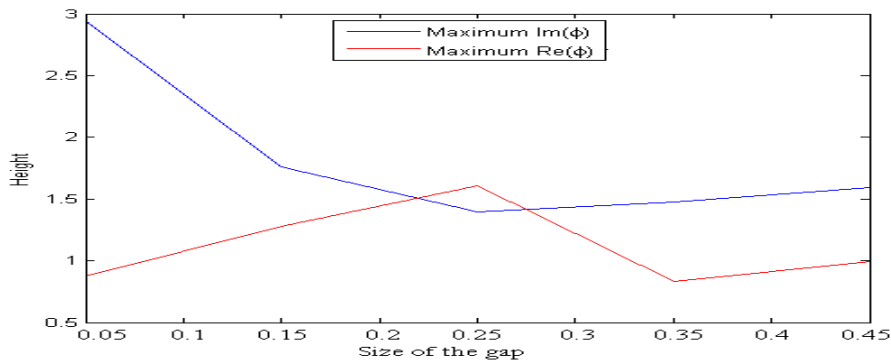
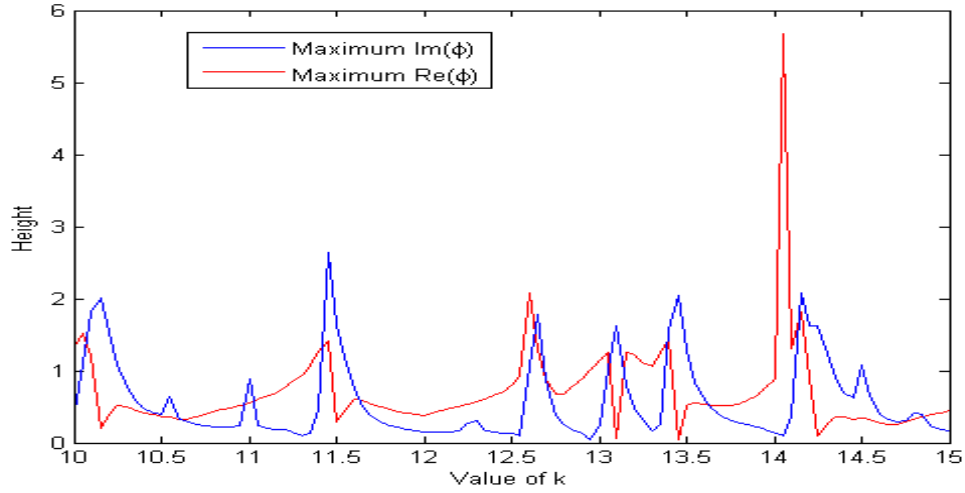


Figure 7.8: Plot of the effect of varying the size of the gap on maximum wave heights

7.3.6 The value of k

Although we have discovered resonant cases by using the model for a closed box, one of the key remaining questions is whether the value of k always has to be evaluated based upon this model in order for resonance to occur. Figure 7.9 shows a graph plotting values of k between 10 and 15 against $\text{Re}(\phi)$ and $\text{Im}(\phi)$. The value of k is plotted for discrete intervals of 0.05, keeping β constant at a value of $\tan^{-1}(\frac{8}{3})$ and $g = 0.05$. There are clear peaks of maximum height, and the values of k for which these occur can be compared to the values of k that are gained by putting integer values of C and D into our eigenfunction (7.1). We hypothesise that these values will closely resemble each other, although they will not exactly match as the latter are based on the closed box problem and the harbour is not entirely closed.

Figure 7.9: Plot of the effect of varying k on maximum wave heights

In Appendix A, k is evaluated for integer values of C and D between one and five. In Table 7.1 below, the values of k from Figure 7.9 where heights of over 1 are achieved for either $\text{Re}(\phi)$ or $\text{Im}(\phi)$ are given, along with proposed matching values of k from the Table in Appendix A. For every peak in the graph plot, there is a proposed value of k

$\text{Re}(\phi)$	$\text{Im}(\phi)$	Proposed
10.05-10.25	10-10.1	10.0580
11.45-11.55	11.35-11.45	11.3272
12.6-12.65	12.6-12.7	12.6642
13.05-13.1	12.95-13.05	12.9531
13.4-13.5	13.15-13.4	13.4209
14.15-14.3	14.05-14.15	14.0496
14.5		14.8189

Table 7.1: Ranges of k where resonance occurs.

that is very close to the actual value of k . This does suggest that the solution to the closed box problem, is the appropriate model to apply when creating resonance in a harbour with a small gap.

In Figure 7.9, the peaks vary in both height and width. This is partly because some of the real peaks where very large wave heights are achieved are being hidden due to the discretisation of k when plotting. Figure 7.10 focuses on k values between 10 and 10.3, plotting for intervals of $\frac{1}{300}$. The shape now changes significantly, and a gradual peak

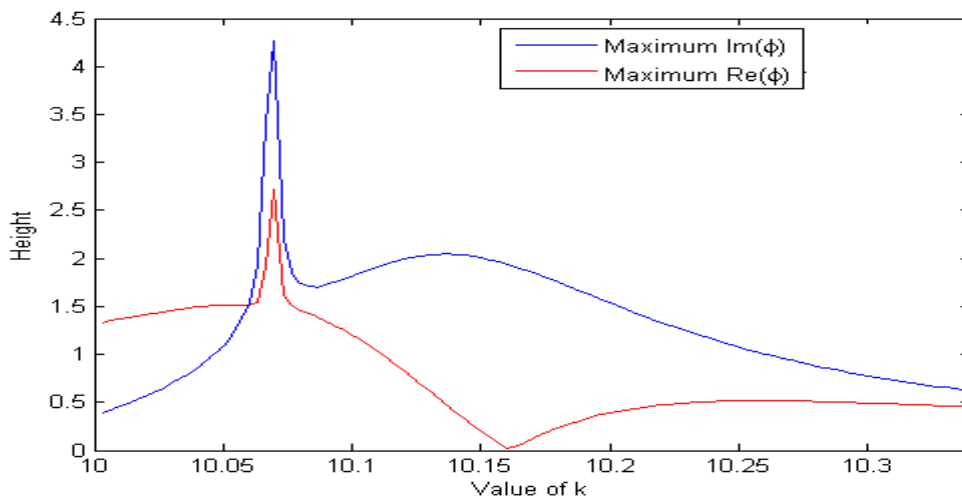


Figure 7.10: Focused plot of the effect of varying k on maximum wave heights.

for the imaginary plot of approximately 2, is distinguished into a sharp peak of over 4 in height, followed by a gradual peak of around 2 (which may well hide yet another sharp peak). By making the value of k more and more accurate, we are getting closer to the very specific values that create strong resonance. This graph shows that only when a very specific value of k is achieved, will large wave heights occur.

Chapter 8

Conclusions

8.1 Summary

In this dissertation we have discussed the work by both Porter [1] and Linton & McIver [2] on the diffraction of water waves around breakwaters. The techniques used in this work have then been applied when modelling the behaviour of waves in a harbour, modelled as a rectangular box that is partially open to the ocean on one side. PDE and Integral Equation techniques have been used to set up expressions describing the wave field both inside and outside of the harbour, and these two expressions were then matched over the harbour mouth where they meet. The resulting integral equation was then solved numerically using Galerkin's method, and issues relating to singularities occurring within the integral equation were discussed and resolved.

A Matlab program was then written to carry out the numerical solution of the integral equation, and the results were then also plotted using Matlab. Evidence of convergence was provided for the harbour solution, and also convergence results for the breakwater problem were found with an adapted version of the harbour program, and these were compared to those of Linton & McIver [2] in order to verify much of the program.

It was then hypothesised that the eigenfunctions required for resonance in a rectangular closed box would also force a resonant response for a harbour where the gap is so small as to almost be a closed box. This was then tested for a gap in the coastal wall that

was one twentieth the width of the harbour. The effect of changing the wave number, the angle of the incident wave, the dimensions of the harbour, and the size of the gap were then analysed. The effect of the wave number was focused on, in order to verify whether resonance only occurred when eigenfunctions based on a resonant response in the closed box were used.

8.2 Future work

8.2.1 The asymmetric gap

Although the asymmetric case has been discussed, there has been no time to actually program this scenario and get any results. The main result that is expected would be that the positioning of focal points for high and low waves would be altered. For example, whereas symmetry along the y axis is currently produced when plotting an incident wave of angle $\beta = \frac{\pi}{2}$, this is unlikely to continue to be the case if the gap is no longer centred within the harbour mouth.

8.2.2 The harbour

Throughout this dissertation, the harbour has been modelled as a simple rectangular box. However very few harbours are actually constructed, or naturally occur in such a shape. Variations in the geometry of the harbour would substantially alter the behaviour of the waves. Cases of resonance would undoubtedly occur for different values of k than have been found for the rectangular case, and might also have different effects within the harbour.

8.2.3 The coastal wall

The model has been set up with the coastal wall extending into the harbour. However, the case where this does not occur also needs to be examined. The mathematical impact of this alteration would be a change to the corner condition (3.27) which has been used to model wave behaviour around the edges of an infinitely thin wedge, rather than a corner.

8.3 Conclusions

The comparison of the contour plots in Chapters six and seven, led us to two main indicators when classifying a resonant case. The first was the comparative amplitudes of the waves inside and outside of the harbour. For non-resonant cases, the maximum heights of the waves outside the harbour are always at least the size of the maximum height within the harbour. The converse is true for the resonant case. The second indicator was the pattern of the contours within the harbour. In the non-resonant case, there is generally just one focal point for maximum wave heights, and the same for minimum wave heights. However for the resonant case, there is a strong alternating pattern between minimum and maximum height waves within the harbour, and the number of these changes in the x and y direction is dependent upon the values of C and D that are used to define the wave number k (7.3).

In order to force a resonant response, it was hypothesised that for a very small gap in the harbour mouth, the behaviour of the waves would be analogous to those in a closed rectangular box of the same dimensions. This was tested by setting the eigenfunction in the solution for ϕ_a to be one that would induce a resonant response in a closed box. Values of the wave number k and the angle of the incident wave β were then evaluated based on the parameters used in this eigenfunction.

In order to analyse the effect of changing the values of k, β, a and g , the maximum wave height within the harbour was found. Using a value of k and β that we predicted to induce resonance, the length a of the harbour was varied, and it was found that making the harbour wider increased the effect of resonance when judged by the maximum wave height within the harbour.

The results for varying β and the gap size g both supported the hypothesis that a harbour with a very small gap would react in a very similar way to a closed box. The largest resonant response was found to occur when β and g were very small, and this response decreased as both these variables were increased. An increase in β would heighten the effect of the incident wave on the harbour, thereby making it less similar to a closed box. Clearly enlarging the gap also reduces the similarity to the closed box

problem. Therefore the results support the hypothesis that resonance occurs within a rectangular harbour with only a small opening onto the ocean, for very similar values of k as for a closed box.

The wave number was then analysed more closely by plotting a range of values of k against the maximum height within the harbour. The values of k which produced a resonant response were all found to be extremely close to values of k which were predicted to induce resonance following the open box analogy. It therefore seems clear that predictions of a resonant response within a rectangular harbour with only a small opening onto the ocean, can be made based upon values of k which would cause a resonant response within a closed box.

Using the knowledge gained about the effect of β and k , a very large response can be forced within the harbour. In Figure 8.1 this has been done by using a value of $k = 14.05$ and $\beta = \frac{\pi}{20}$. From the table in Appendix A, it can be seen that there is a value of $k = 14.0496$ ($C = 4, D = 4$) given for resonance in the closed box which is extremely close to this choice for k . As stated earlier, the selection of an extremely small angle β most effectively mimics the closed box case. The result of these choices for k and β is to force a disastrously strong resonant response within the harbour.

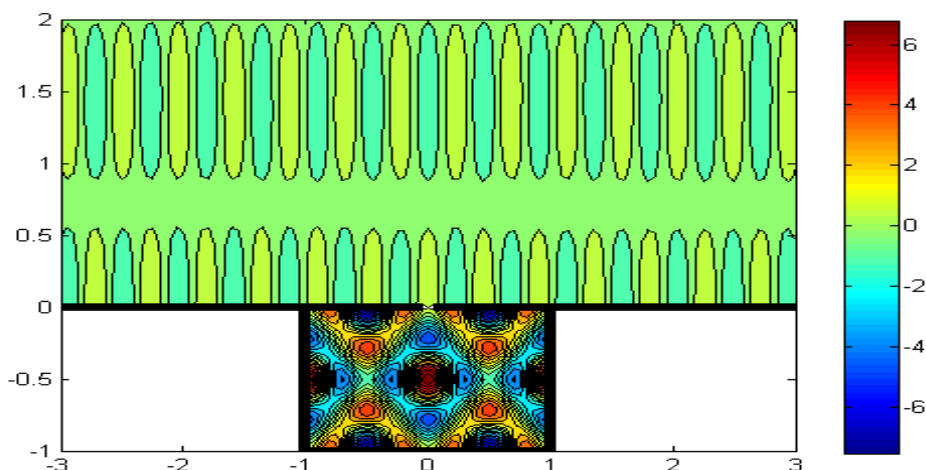


Figure 8.1: Plot of $\text{Re}(\phi)$ showing resonant response in the harbour, with $k = 14.05$ and $\beta = \pi/20$.

Appendix A

Values of k

C	D	k	C	D	k
1	1	3.5124	4	1	12.6642
1	2	4.4429	4	2	12.9531
1	3	5.6636	4	3	13.4209
1	4	7.0248	4	4	14.0496
1	5	8.4590	4	5	14.8189
2	1	6.4766	5	1	15.7863
2	2	7.0248	5	2	16.0190
2	3	7.8540	5	3	16.3996
2	4	8.8858	5	4	16.9180
2	5	10.0580	5	5	17.5620
3	1	9.5548			
3	2	9.9346			
3	3	10.5372			
3	4	11.3272			
3	5	12.2683			

Table 1: Values of k given various values of C and D .

Bibliography

- [1] D. PORTER BSc PhD, *Wave diffraction around breakwaters* Report No IT 200, December 1979.
- [2] C.M. LINTON & P McIVER, *Handbook of Mathematical Techniques for Wave/Structure Interactions* Chapman & Hall CRC 2001.
- [3] A.JANSA, S.MONSERRAT AND D.GOMIS, *The rissaga of 15 June 2006 in Ciutadella (Menorca), a meteorological tsunami* Advances in Geosciences, 12, 1-4, 2007.
- [4] Scripps Institution of Oceanography, UC San Diego, http://earthguide.ucsd.edu/earthguide/diagrams/waves/swf/wave_seiche.html
- [5] ABRAMOWITZ and STEGUN, *Handbook of Mathematical Functions* electronic copy at <http://www.math.sfu.ca/~cbm/aands/>
- [6] WOLFRAM MATHWORLD, <http://mathworld.wolfram.com/topics/BesselFunctions.html>
- [7] D. PORTER and D. STIRLING, *Integral equations a practical treatment, from spectral theory to applications* CUP 1990
- [8] R. KRESS, *Linear Integral Equations* Applied Mathematical Sciences Volume 82, 2nd ed. Springer-Verlag 1999.
- [9] A.RABINOVICH and S.MONSERRAT, *Generation of Meteorological Tsunamis (Large Amplitude Seiches) Near the Balearic and Kuril Islands* Kluwer Academic Publishers 1998.
- [10] S.C.WILDE and A.T.PEPLow, *A Boundary integral equation formulation for the Helmholtz equation in a locally perturbed half-plane* June 2002.